Evaporative Cooling of Sodium Atoms

by

Kendall Bruce Davis

B.A. Physics, Middlebury College (1990)

Submitted to the Department of Physics in
partial fulfillment of the requirements
for the degree of

Doctor of Philosophy

at the

Massachusetts Institute of Technology

May, 1995

Signature of the Author

Department of Physics
May, 1995

Certified by

Wolfgang Ketterle
Assistant Professor of Physics
Thesis Supervisor

Accepted by

George F. Koster
Chairman, Department Committee
on Graduate Studies

Evaporative Cooling of Sodium Atoms
by
Kendall B. Davis

Results of experiments on evaporative cooling of sodium atoms are presented. Atoms are loaded into a spherical quadrupole magnetic trap and are cooled by a novel technique, rf induced evaporation. The elastic collision cross section for cold sodium atoms is measured to be 6 10^{-12} cm^2. These initial experiments result in an increase of phase space density of 190. Further cooling is impeded by Majorana spin flips at the trap center.

A novel optically plugged magnetic trap is developed which does not suffer from the Majorana spin flips and further evaporation results in an additional increase in phase space density of 500, mainly limited be the spatial resolution of the detection imaging system.

A modified optically plugged trap (a light sheet trap) is demonstrated which circumvents the diagnostic problems. In this trap evaporation was shown to increase phase space density by an additional factor of 5, the final phase space density is within one order of magnitude of that required to reach Bose Einstein condensation. Further progress is anticipated in the near future.

Thesis Supervisor: Wolfgang Ketterle
Title: Assistant Professor of Physics

Contents

List of Figures

Chapter 1
Introduction

Over the last several years there have been tremendous advances in the area of trapping and cooling of neutral atoms. These advances are motivated by a desire to control the motion of atoms to the greatest extent possible. Researchers are also hopeful that very cold atomic samples will lead to the observation a Bose-Einstein condensate in a dilute gas. The signature of Bose-Einstein condensation is the macroscopic population of the trapping potential's ground state.

The prediction that a cold dense sample of bosons will condense relies on only a few very simple assumptions.

1) All particles are indistinguishable

2) There is no limit to the number of particles that can occupy a given quantum state

3) The particles are most likely to be in a state that maximizes the entropy of the system.

These reasonable assumptions lead to a rather surprising result, that below a certain critical temperature the entropy of the system is maximized by having a macroscopic fraction of the population in the ground state. It has been predicted that a Bose Condensate will exhibit some unusual behavior, such as a total lack of viscosity and a nearly infinite heat conductivity similar to liquid He II[1]. Also it is anticipated that a Bose condensate will react in an unusual way when exposed to laser light. There are predictions that a condensate will have an increased linewidth for light absorption, there are also predictions that a Bose condensate might reflect all incident radiation[2, 3]. The exciting thing is that these questions will not be resolved until a Bose condensate is formed and studied.

If a Bose condensate generated in a trap could be released into free space it would form a freely propagating coherent matter wave. There is an excellent analogy between such a source of coherent atoms and a freely propagating laser beam. In fact atomic physicists have already dubbed such a source a "Boser".

There is no doubt that a Boser would find a use in a broad variety of applications. Potential applications might include improved atomic clocks, and atom interferometers. A Boser might be used instead of a conventional thermal atomic beam for direct write lithography. A coherent source of atoms can be focused more tightly allowing smaller patterns to be mapped out. This could be useful to the computer industry which is always in search of ways to make features on chips smaller.

Given such a variety of interesting scientific goals on the horizon it is not surprising that we are not the only group pursuing Bose condensation. Indeed there has been fabulous progress in many different groups using many different atoms. The group which has always been the closest to observing Bose condensation, is that of Tom Greytak and Dan Kleppner at MIT. This group works with atomic hydrogen and has done the pioneering research that has established a number of techniques including evaporative cooling. Evaporative cooling requires the selective removal of the atoms in the trap that have the highest total energy. Elastic collisions among the remaining atoms repopulates the high energy tail of the Maxwell Boltzmann distribution. When this rethermalization is complete the temperature has decreased. Therefore an important prerequisite for evaporation is that the elastic collision rate for atoms in the trap be high in comparison to the rate at which atoms are being lost due to background gas collisions. The elastic collision rate is equal to the product of the density, the thermal velocity and the elastic collision cross section.

Atomic hydrogen has several attractive features as well as some experimental drawbacks. On the positive side, hydrogen is a simple system theoretically and virtually all processes regarding its atomic interactions can be calculated exactly. Hydrogen can also be

loaded into a trap without using lasers and thus experiments using hydrogen are free from some of the technical difficulties associated with lasers.

Hydrogen has a relatively small elastic collision cross section. Therefore higher densities and thermal velocities are required to evaporatively cool hydrogen. This is a drawback because trapped atoms suffer from a density dependent loss process (dipolar relaxation) which for atomic hydrogen can be a dominant loss process. Probably the biggest drawback in working with hydrogen is that hydrogen traps work only with techniques involving liquid helium. This means that the trapped atoms are relatively inaccessible. This handicap has probably prevented the hydrogen trappers from observing a Bose condensate for several years. For a complete discussion on the experiments involving hydrogen see John Doyle's thesis[4].

There has also been an incredible amount of work using alkali atoms. Alkali atoms can not be loaded into magnetic traps by the techniques used for hydrogen. However unlike hydrogen, alkali atoms have strong optical transitions at wavelengths that are accessible to commercial laser systems. For these reasons a number of techniques for cooling and trapping alkalis have involved laser light. In fact, laser cooling and trapping has generated so much interest that it has developed into an independent subfield of atomic physics.

The biggest breakthrough in laser cooling of alkali atoms came with the invention of the Magneto-Optical Trap, or MOT for short[5]. This trap is used by virtually all groups trapping and cooling alkali atoms because it is easy to set up, has a wide velocity capture range, and is relatively insensitive to misalignment. This trap is used by most groups as an effective way to collect a large number of cold atoms. These atoms can then be cooled further by optical techniques such as Polarization Gradient cooling [6]

One drawback of using light to cool atoms is that the energy released from a single photon recoil sets a limit to the lowest temperature that optical techniques can easily reach. Some optical techniques[7-9]. have managed to beat the recoil limit but have not been

demonstrated at high densities. This is the real challenge of Bose condensation: you must achieve high densities as well as low temperatures.

The success of evaporative cooling in atomic hydrogen led many groups to pursue evaporation with alkalis. The challenge associated with evaporatively cooling alkali atoms is that evaporation requires relatively high atomic densities and the trapping and cooling techniques available until recently only worked well at relatively low atomic density. The gap was bridged with the invention of the Dark SPOT trap[10]. The Dark SPOT trap is a modified version of the MOT. Atomic densities two orders of magnitude higher than those achieved in the MOT have been observed in the Dark SPOT (with a similar number of atoms). A detailed description of the Dark SPOT can be found in Mike Joffe' s thesis[10]. A brief description of the Dark SPOT will be given in Chapter 2.

The Dark SPOT has become the method of choice for collecting a large number of atoms in a dense sample. Once a sample is obtained it must be loaded into a conservative potential so that it can be evaporatively cooled. In a conservative potential an atom's distance from the minimum of the potential depends on its energy. Thus, an atom discarded on the basis of position from the minimum is also being discarded on the basis of energy which, as was pointed out earlier, is a prerequisite for evaporation.

Currently there are two distinctly different conservative potentials in use. One is generated by an atoms interaction with static magnetic fields (a magnetic trap). The other is generated by an atoms interaction with intense laser light (a dipole trap). We have chosen to work with a magnetic trap because dipole traps require intensities that can only be achieved by focusing the laser beam tightly. Atoms in dipole traps are confined to the region of high laser intensity and thus these traps have a very small volume. This is a disadvantage because we are loading the trap with a sample of fixed density and thus a smaller volume means fewer atoms. In our magnetic trap we have confined more than 10^9 atoms in comparison to roughly 10^4 in a dipole trap. The magnetic field configuration we

have chosen, the spherical quadrupole is attractive because it confines atoms tightly and allows us to evaporate quickly.

Once these atoms are loaded into the magnetic trap we adiabatically increase the trapping potential. This increases the density and the temperature of the atomic sample, and therefore the elastic collision rate. Next we evaporate the sample using a novel technique, rf induced evaporation. In our initial experiments we increased the phase space density of our trapped sample by a factor of 190. In addition we measured the elastic collision cross section for sodium which we found to be $6\ 10^{-12}\ cm^2$.

At this point further cooling became impossible because of a temperature dependent loss process in our trap. The spherical quadrupole trap has a zero of the magnetic field in the trap center. Atoms can be lost from the trap if they come too close to the origin. As the trapped sample cools it occupies less volume and thus the loss rate increases with decreasing temperature.

Our solution to this problem was to use the dipole potential mentioned earlier to prevent atoms from being lost from the trap. The dipole potential can be either attractive (as is the case when it is used as a trap) or repulsive depending on whether the laser is tuned below or above the atomic resonance. We are using a repulsive dipole potential to keep atoms away form the trap center, thus preventing them from being lost.

This combined magnetic and dipole force potential creates a novel trapping geometry that has most of the advantages of the magnetic quadrupole trap without the disadvantages. We have called this new trap the optically plugged magnetic quadrupole trap because the tightly focused laser beam effectively "plugs" the "hole" in the magnetic quadrupole trap. Using this new trapping geometry we have increased the phase space density of atoms in our trap by another factor of 500. At this point our phase space density was still a factor of 40 lower than that required for Bose condensation.

Although the optically plugged magnetic quadrupole trap works extremely well, it can be difficult to determine the atoms temperature and density in this trap. The reason is that

as the atoms cool they occupy less volume and eventually the trapped sample becomes smaller than our diffraction limited optical system can resolve. This could be easily remedied by adiabatically decompressing our potential and thus increasing the volume the trapped sample occupies.

Unfortunately adiabatic decompression became very difficult because our trapping coils move in an uncontrollable way as we decompress and thus the optical plug becomes misaligned. To solve this problem we developed a modified version of the optically plugged trap where we plug the hole with a laser beam that has a five to one aspect ratio in its cross section. This type of laser focus, usually referred to as a light sheet, allowed us to displace the atom cloud away from the trap center. Atoms were then much less sensitive to the position of the field zero and adiabatic decompression became trivial.

Initial experiments with this new trap were encouraging. We were able to decompress our cloud and obtain a sample with a density of $3\ 10^{12}$ cm^{-3} and a temperature of 1 μK. Incidentally this temperature is a factor of three below the photon recoil limit mentioned earlier as a limitation to cooling schemes involving light. This combination of density and temperature yields a phase space density which is only a factor of 10 lower than that required for Bose-Einstein condensation. This result is comparable to the best hydrogen result (a factor of 5 away from BEC) in terms of closest approach to Bose condensation. There is much hope that in the near future we will be able to cross the transition line.

Chapter 2
Combining Laser Cooling with Evaporation

Evaporative cooling was a breakthrough in the quest for higher phase space densities in alkalis. As was discussed in chapter 1, alkali atoms have several advantages over atomic hydrogen in terms of experimental ease and elastic collision cross section. A crucial prerequisite for evaporation of alkalis was obtaining a dense sample in a light trap. To achieve this goal we developed the dark SPOT trap. Atoms in this trap have densities two orders of magnitude higher than conventional light traps with a similar number of atoms and this trap is currently used by all groups doing evaporation in alkalis[11-13].

Atoms that are confined in the Dark SPOT trap have a temperature on the order of 1 mK. We have been able to drastically reduce the temperature of these atoms by employing a new cooling scheme, dark polarization gradient molasses. During the cooling atoms are not trapped, they are only confined by the viscous force of the molasses. It is important that the cooling time be relatively short so that the atomic density is not diminished while the atoms are cooled. Temperatures of 100 μK are attainable with a few ms of cooling. Both of these techniques are described in detail in Mike Joffe's thesis[10]. My motivation is to highlight these techniques which were crucial to the success of our current experiment.

2.1 The Dark SPOT and Dark Cooling

The Magneto-Optical Trap (MOT)[14] revolutionized the field of neutral atom trapping and cooling when it was introduced in 1987. This trap has a wide velocity capture range, and can hold many atoms at fairly high densities. An atom in the MOT which is displaced from the trap center will preferentially absorb trapping light directed towards the center and undergo spontaneous emission isotropically. Therefore, this atom experiences a net force toward the trap center.

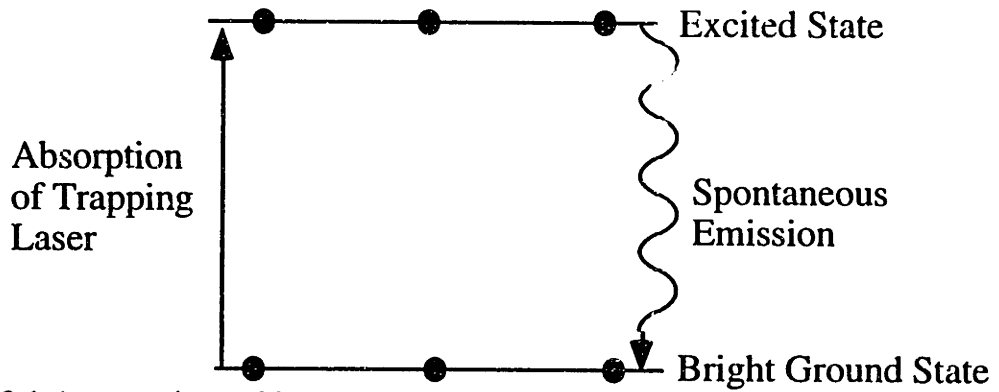

Figure 2.1 Atoms, pictured here as dark circles, confined in the MOT spend about half of their time in the ground state and half of there time in the excited state.

The MOT however does have some limitations. If one atom in the trap scatters a photon and another atom absorbs that photon, then the two atoms experience an effective repulsive force. This repulsive force becomes comparable to the force which confines the atoms at densities in excess of 10^{10} cm^{-3}.

The Dark SPOT trap offers a clever way of circumventing this repulsion. Atoms in the Dark SPOT trap spend the majority of the time in a dark ground state that does not interact with the trapping light. They experience the force of the trapping light only with a reduced duty cycle (see figure 2.2). This reduced trapping force is still sufficient to keep them confined.

This same technique of shelving atoms to avoid the problems associated with high densities can also be applied to polarization gradient cooling. A potential drawback to this approach is that the cooling requires significantly more time because of the atom's reduced duty cycle in the cooling light. However, as a practical matter, this does not present a problem because 10^{10} atoms can be cooled to 100 μK in about 3 ms. During that 3 ms the atoms are confined viscously in the molasses and very little density is lost.

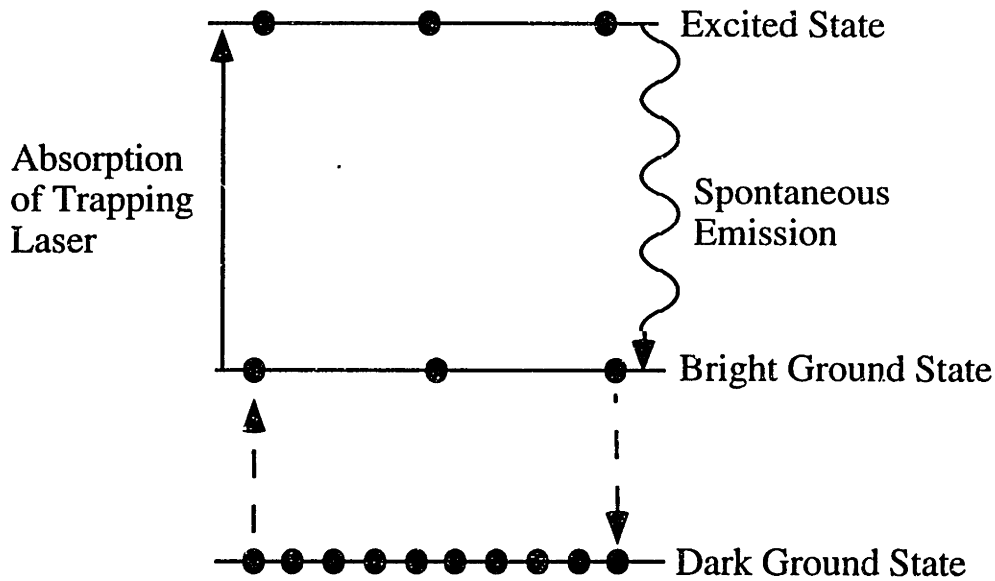

Figure 2.2 Atoms in the dark SPOT trap spend the majority of their time in the dark ground state and are only occasionally cycled into the bright ground state. Atoms that are in the bright ground state feel the full trapping force, and the density of these atoms is about 10^{10} cm^{-3} as in the MOT. However the total density including atoms in the dark state is about 10^{12} cm^{-3}.

In sodium the dark ground state is the (3S) F=1 state, the bright ground state is the (3S) F=2 state and the excited state is the ($3P_{3/2}$) F=3 state. Transfer of atoms between the bright ground state and the dark ground state is accomplished by optical pumping via the ($3P_{3/2}$) F=2 state.

2.2 Magnetic Trapping

There are several excellent discussions of magnetic trapping in the literature [15, 16, 17] and the goal here is to give a brief argument for how a magnetic trap works without delving into optimized geometries and other details which are covered elsewhere. Magnetic traps can be understood using only classical mechanics (in fact you can magnetically trap a macroscopic permanent magnet[18]).

Consider a magnetic dipole, μ in an external magnetic field, B. The energy of this dipole is

$$E = -\vec{\mu} \cdot \vec{B}.$$

At first glance it seems all we have to do to make a trap (a global minimum in the potential) for such a dipole is to create a magnetic field that has a global maximum. Unfortunately

Maxwell's equations forbid such a maximum[15]. We can however make a local minimum in the magnitude of the magnetic field. For instance the following field, called a spherical quadrupole, has a minimum at the origin and also satisfies Maxwell's equations

$$\vec{B} = B'\{-x,-y,2z\}.$$

The only way to confine a dipole in such a field would be to keep the dipole oriented antiparallel to the local magnetic field direction. For such a dipole the potential would be

$$U = \mu B'\sqrt{x^2 + y^2 + 4z^2}$$

Recall, however, that this dipole would experience a torque equal to

$$\vec{\tau} = \vec{\mu} \times \vec{B}.$$

which would orient the dipole along the direction of magnetic field.

If however if the dipole has an angular momentum L, antiparallel to the direction of μ (see figure 2.1), then this torque will change the angular momentum in the following way

$$\vec{\tau} = \frac{d\vec{L}}{dt}.$$

Because L is antiparallel to μ the torque is orthogonal to L, and changes the direction of L without changing its magnitude. The result is that L precess around B with frequency ω, where ω satisfies the following equation

$$\vec{\tau} = \vec{\omega} \times \vec{L}.$$

Hence ω has a magnitude of μB/L and is antiparallel to B.

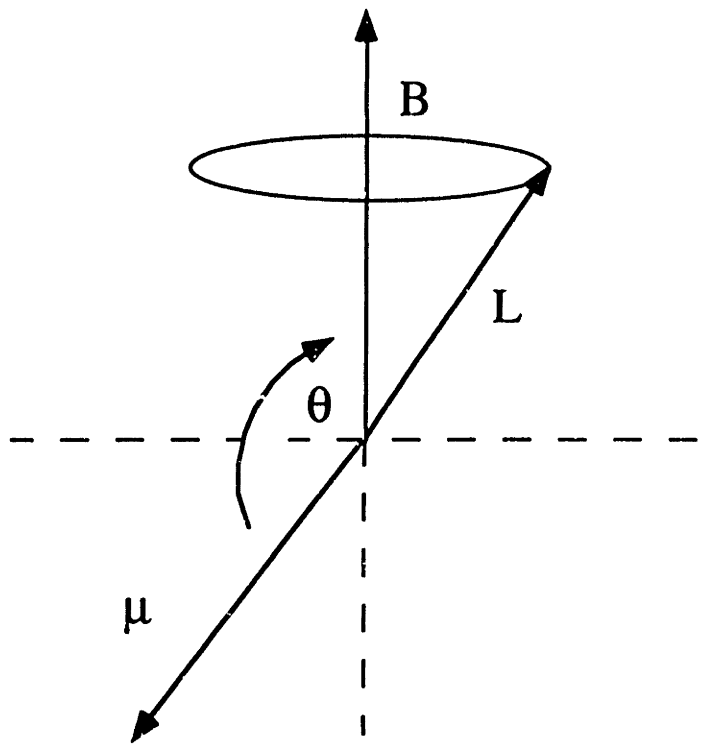

Figure 2.3 A magnetic dipole with angular momentum L in an external magnetic field B precesses around B with frequency ω.

Although the dipole could lower its energy by being oriented along the same direction as the field it is stable in its nearly antiparallel orientation because of the angular momentum. If the direction of the magnetic field were to change slowly with respect to the precession frequency then the dipole would adiabatically follow the field and the relative orientation of the dipole and the field would remain unchanged. Therefore a dipole with angular momentum would be confined in the spherical quadrupole magnetic field described above.

Fortunately the sodium atom, and every other atom with an unpaired electron, has just the properties that we would like. It has a permanent magnetic dipole moment and has angular momentum. Sodium is trapped in its ground state because its excited states are relatively short lived (16 ns is the lifetime of the first excited state). Sodium has a nuclear spin I=3/2 and an electronic spin J=1/2. These two spins can couple to form a total angular momentum F=1 or F=2. These two states are separated by an energy E with E/h =1.7

GHz. In practice we call both of these states the ground states because they are both part of the 3S electronic state.

Sodium therefore has a total of eight magnetic hyperfine ground states (see figure 2.4). Only a the states F=2,m_F=2, F=2,m_F=1 and F=1,m_F=-1 can be trapped magnetically: these states are weak field seeking (dE/dB > 0) thus for these states the magnetic moment of the atom is nearly antiparallel to the magnetic field. Due to a high collisional loss rate it is impractical to trap the F=2,m_F=1 state[19, 20]..

In general an atom's energy as a function of magnetic field (for low magnetic fields) is given by

$$E = gm_F\mu_B B.$$

where μ_B is the Bohr magneton and g is that particular state's g factor. The F=2 state has a g factor equal to 1/2 and the F=1 state has a g factor equal to -1/2.

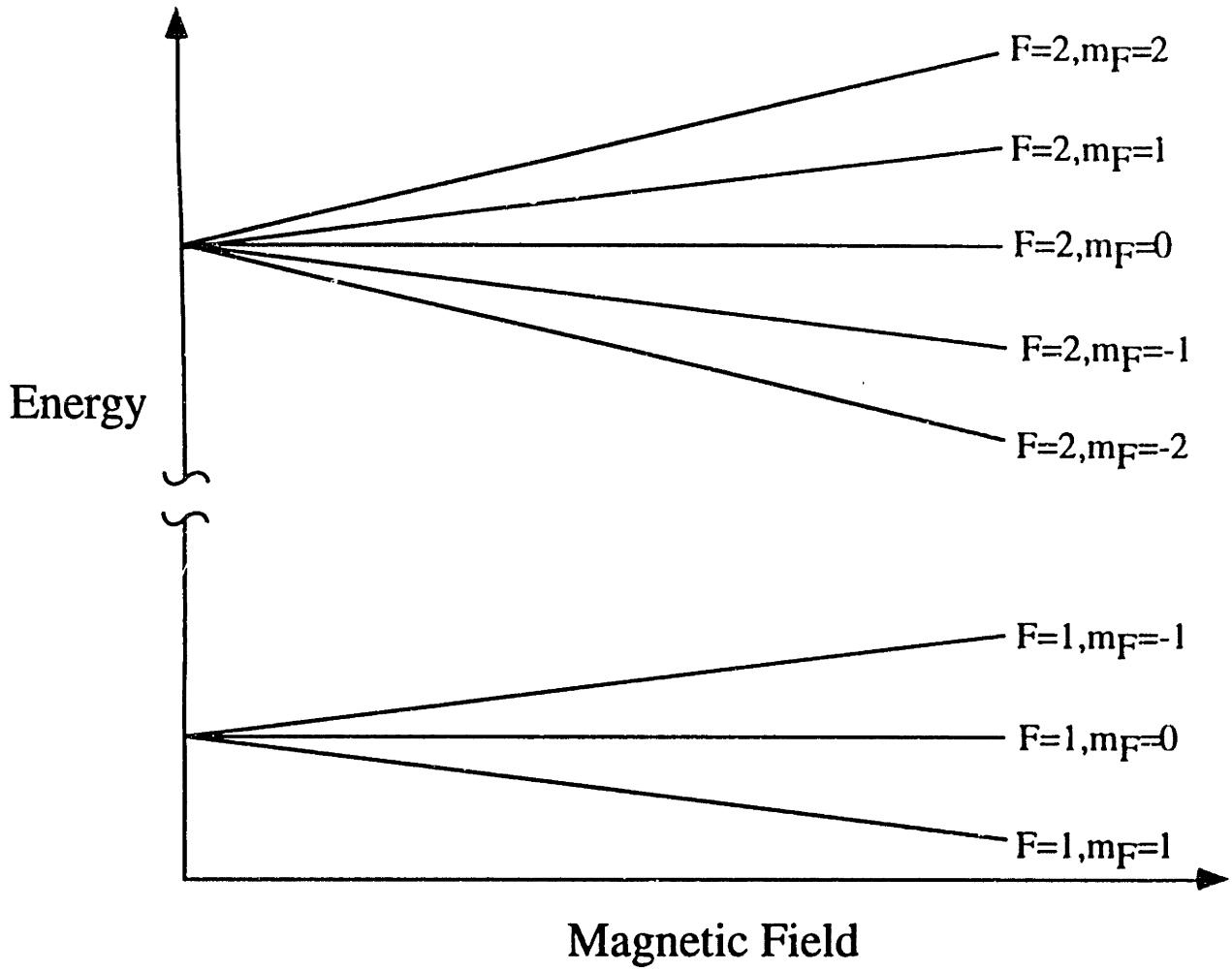

Figure 2.4 Hyperfine energy vs. magnetic field for the F=1 and F=2 ground states of sodium.

In our experiment we trap the F=1, m_F=-1 state. This state is chosen because it is the most convenient to trap. Most of our atoms are in the F=1 state after dark cooling, thus by quickly ramping up a magnetic field we can catch all of the F=1, m_F=-1 atoms in our magnetic trap. Naturally without any optical pumping only 1/3 of the atoms happen to be in this state.

The trapping field is generated by a pair of anti Helmholtz coils. When loading our magnetic trap it is important to offer the atoms a potential which is not too steep (which would cause heating), nor too shallow (which would result in a loss in density). We have designed our trapping coils so this catching field is only one tenth of the maximum field.

This allows us to adiabatically compress the atomic cloud after we load them into the magnetic trap. Adiabatic compression will be discussed in more detail in Chapter 3.

Chapter 3
Forced Evaporation

Forced evaporative cooling in my opinion is, one of the simplest cooling schemes for neutral atoms. Originally proposed by Hess [21] and first realized by Masuhara et al. [22] evaporative cooling is also well matched for the pursuit of high phase space densities. Many optical cooling schemes can cool below the single photon recoil limit but have not been demonstrated at high densities. Evaporative cooling requires high density and if done appropriately can lead to increasing density as the temperature decreases, despite a loss of atoms.

Any cooling scheme that increases phase space density must remove entropy from the atomic sample. In optical cooling schemes the atom undergoes a spontaneous decay as a result of which entropy leaves with the photon. In evaporative cooling entropy leaves with the atom.[23]

Evaporative cooling works by removing the highest energy atoms from a thermal (Maxwell Boltzmann) distribution. Elastic collisions among the remaining atoms repopulate the high energy tail of the Maxwell Boltzmann distribution. The new thermal distribution has a lower average energy per particle (temperature) than the original distribution. If this process is repeated by continuously lowering the threshold for evaporation it is called forced evaporation (see Figure 3.1).

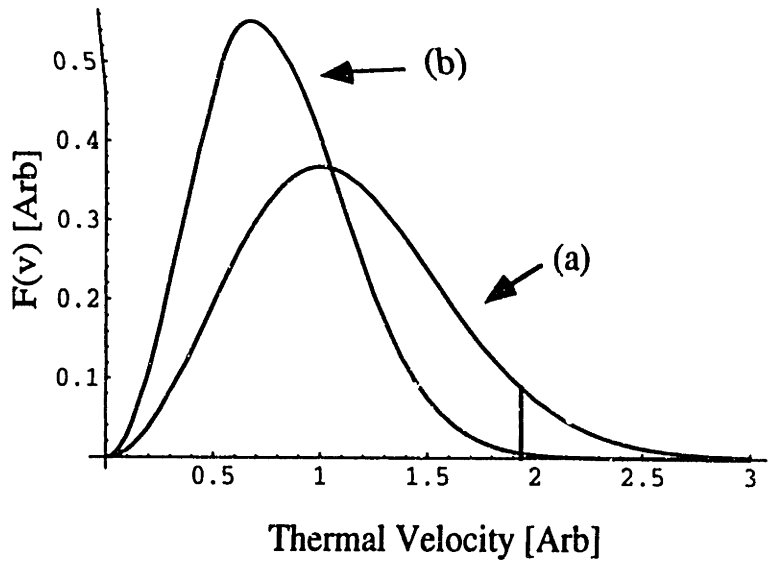

Figure 3.1 (a) The original Maxwell Boltzmann distribution is truncated and the high energy tail is discarded. (b) When the remaining atoms rethermalize they repopulate the high energy tail and the cloud has a reduced temperature. (Note the effect has been exaggerated for clarity, the picture shown would actually correspond to about 7 truncation and thermalization steps.)

There are several key ingredients to achieve forced evaporation in a trapped atomic sample. The most basic requirement is that the elastic collision rate must be much greater than the loss rate of atoms due to background gas collisions. Adiabatic compression is a method to increase the elastic collision rate of a sample, and has been important for initiating evaporation. Whether or not the elastic collision rate increases as the sample cools depends critically on the trapping geometry used, thus the choice of the trapping is an important one. Finally, in order to force the evaporation a method must be employed to lower the depth of the trapping potential so that atoms with the highest average energy can escape.

3.1 Adiabatic Compression

As a sample is being compressed its elastic collision rate increases due to higher densities and higher temperatures. How the density and temperature change is a function of the trapping potential used. The following argument demonstrates that a linear potential is superior for adiabatic compression.

The magnitude of a magnetic potential generated by a trap coil of radius R at a distance of d from the center of the trap is equal to,

$$U(d) = \mu B_0 \left(\frac{d}{R}\right)^n$$

where n is the order of the potential, μ is the magnetic moment of the atom, and B_0 is the magnetic field near the coils. Thus to confine a sample of atoms with radius d and temperature T the following condition must be satisfied,

$$kT = \mu B_0 \left(\frac{d}{R}\right)^n.$$

In order to insure optical access to our trapped sample it is necessary that R be much greater than d (typically R = 30d). Therefore we can minimize the necessary B_0 by using a linear potential, or with the same B_0 required to confine the cloud in a quadratic potential we can adiabatically compress the cloud in a linear potential.

The following argument gives the dependence of the elastic collision rate on the field gradient in a linear potential. If we define $\langle r \rangle$ as a particles average distance from the center of trap, then the virial theorem provides the following relationship between $\langle r \rangle$ and the temperature.

$$\langle U \rangle = \mu B' \langle r \rangle = 3kT$$

Notice that a particles average distance from the center of the trap is also related to the density in a simple way

$$n \propto \frac{1}{\langle r \rangle^3}.$$

Any process which is adiabatic must have the following relationship between density and temperature.

$$\frac{n}{T^{\frac{3}{2}}} = constant$$

Combining these equations we get that $n \propto B'$ and that $v_{Th} \propto \sqrt{T} \propto (B')^{\frac{1}{3}}$ where v_{th} is the thermal velocity . The elastic collision rate is proportional to the product of density and the thermal velocity and therefore

$\Gamma_{el} \propto (B')^{4/3}$.

There is a natural limit to how much an atomic sample can be adiabatically compressed; higher gradients require higher currents, which in turn require higher power. To my knowledge we have pushed this technology harder than any other group in the field. We currently run 300 Amps through our coils dissipating 6000 Watts inside a UHV vacuum system with a base pressure of 3 x 10^{-11} Torr. As a result of this effort we are able to increase our elastic collision rate by a factor of 20 by increasing our gradient by a factor of 10.

3.2 Optimized Trapping Geometries For Evaporation

The dynamics of evaporative cooling depend critically of the shape of the trapping potential used. In order for evaporation to be sustainable the atomic sample must contract enough as it cools that the density is increasing despite the loss of atoms. A more stringent requirement, and in practice a more important one, is that the elastic collision rate is increasing as the sample is cooled. The elastic collision rate is proportional to the density times the thermal velocity, thus for the collision rate to be increasing the density must be increasing faster than the thermal velocity is decreasing.

In principle any magnetic field configuration that has a local three dimensional minimum in the magnitude of the magnetic field could be used as a trap for atoms in a weak field seeking state. The challenge is to find a configuration that offers the greatest increase in elastic collision rate as the atomic sample cools. The linear potential is advantageous for adiabatically compressing the sample and as we will see it is also essential for the evaporation process to be self accelerating.

The density of atoms with a temperature T in a three dimensional potential $U = r^m$ is proportional to

$$n \propto \frac{1}{T^{3/m}}$$

The elastic collision rate is therefore proportional to

$$\Gamma_{el} \propto \frac{N(T)}{T^{3/m-1/2}}$$

where N(T) is the number of atoms in the trap at a given temperature. Recall that as we evaporate we loose atoms and atoms are also being lost due to background gas collisions. To maximize Γ_{el} m should be made equal to one (a linear potential). A more detailed argument, explicitly solving for N(T) in various potentials, is given in the appendix to chapter 3.

3.3 RF Induced Evaporation

As was outlined in section 2.3 we trap atoms in the F=1, m_F=-1 hyperfine state. In this state the atom' s energy increases linearly as a function of magnetic field. Recall that we are using the spherical quadrupole trap which has a magnetic field as a function of position $\vec{B}(x,y,z) = B'\{-x,-y,2z\}$.

This means that the atoms energy increases linearly as a function of position from the origin. The splitting between a sodium atom's hyperfine levels as a function of position is shown in figure 3.2.

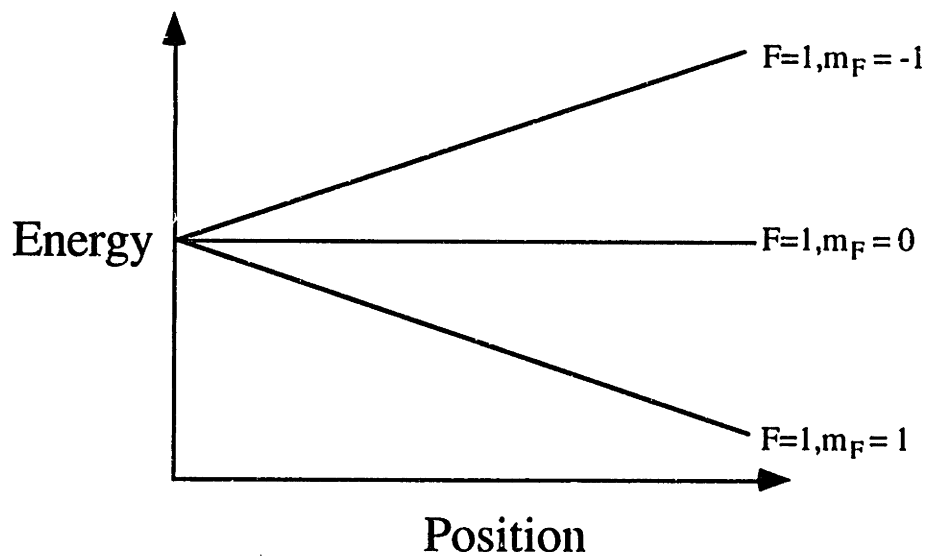

Figure 3.2 Hyperfine energy states of the F=1 manifold as a function of displacement from the origin in a spherical quadrupole trap.

As was pointed out earlier evaporation requires the selective removal of atoms with the highest total energy. Atoms with the highest total energy sample the highest magnetic fields and as a result have the greatest separation between their magnetic hyperfine levels. One convenient way to remove these atoms from the trap is to expose them to resonant radiation which drives the atoms to one of the other two magnetic hyperfine levels. By this method we can selectively remove atoms because the linewidth of these rf transitions is completely negligible in comparison to thermal energies. In this case the resonance frequency is typically in the MHz (rf) domain. By lowering the frequency of the rf we can discard atoms of lower energy, see fig 3.3.

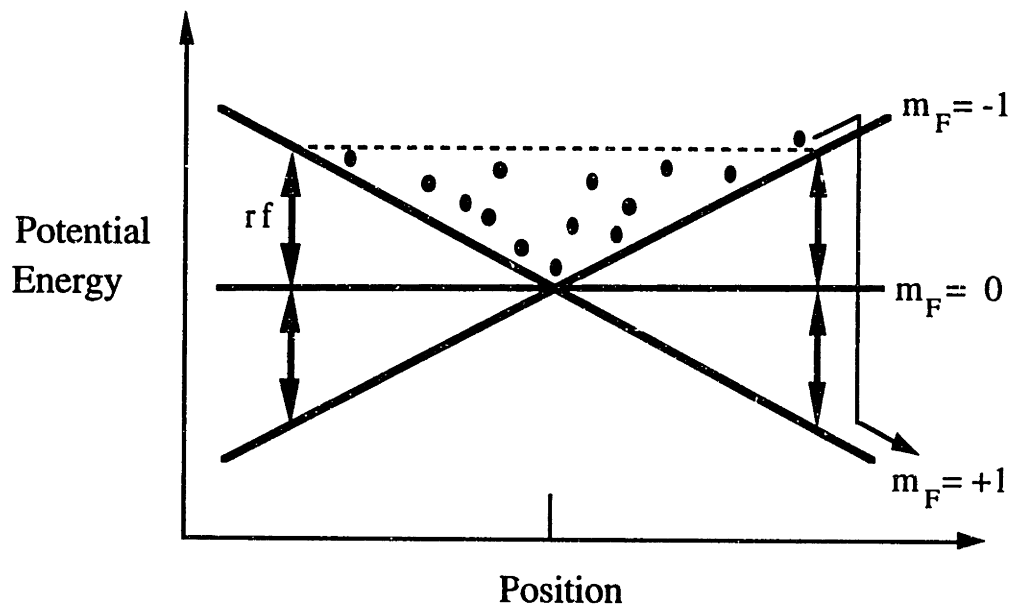

Figure 3.3 Energy levels of sodium vs. displacement from the origin for a spherical quadrupole trap. The rf radiation selectively removes atoms from the trap which are in resonance. By decreasing the frequency lower energy atoms can be removed.

In the following section we will develop a formalism for describing the atom's interaction with the rf and the static trapping field using the dressed atom approach. In this formalism the rf is treated as a linearly polarized quantum mechanical field. The results of this calculation are only strictly valid if the atom is at rest. In practice the results can be extended to atoms moving slowly enough that the rate of change their potential energy

divided by h is small in comparison to the square of the rf Rabi frequency. This is the requirement for an atom to adiabatically follow the energy eigenstates derived below.

The Hamiltonian for an atom interacting with a static external magnetic field and a quantized rf radiation field has three parts, the atomic Hamiltonian H_A, the radiation Hamiltonian H_R and the interaction Hamiltonian V[24]. The atomic Hamiltonian is a result of the atom's magnetic moment interacting with the static external magnetic field;

$$H_A = -\vec{\mu} \cdot \vec{B}_0.$$

The Hamiltonian for the radiation field is given by the well known expression for a harmonic oscillator

$$H_R = \hbar \omega a^+ a.$$

The quantities a and a^+ are the raising and lowering operators for the field.

The interaction Hamiltonian is the result of the atom's magnetic moment interacting with the time dependent magnetic field of the photon and has the following form

$$V = -\vec{\mu} \cdot \vec{B}_R.$$

Expressing the magnetic field of the photon in terms of raising and lowering operators is covered in detail in reference.24 and we will simply quote the result here

$$V = \hbar\lambda\left[\left(\hat{e} \cdot \vec{F}\right)a + \left(\hat{e}^* \cdot \vec{F}\right)a^+\right].$$

F is the total (nuclear plus electronic) angular momentum of the atom. Lambda has units of frequency and is proportional to $1/L^{3/2}$ where L is the characteristic length of the quantization volume. The unit vector $\hat{e}$ is the polarization vector of the rf magnetic field, taken to be linear.

The static magnetic field of the spherical quadrupole trap changes direction as a function of position, whereas the polarization of the rf field is a constant. It is most convenient to work in the coordinate system where the local static magnetic field is along the z axis. In this coordinate system the rf polarization is a function of position (see fig. 3.4). For convenience of notation we let $\hbar$ equal one and define $\omega_0 = \frac{\mu B}{\hbar}$, which is the atom's precession frequency as derived in section 2.3. The Hamiltonian is then

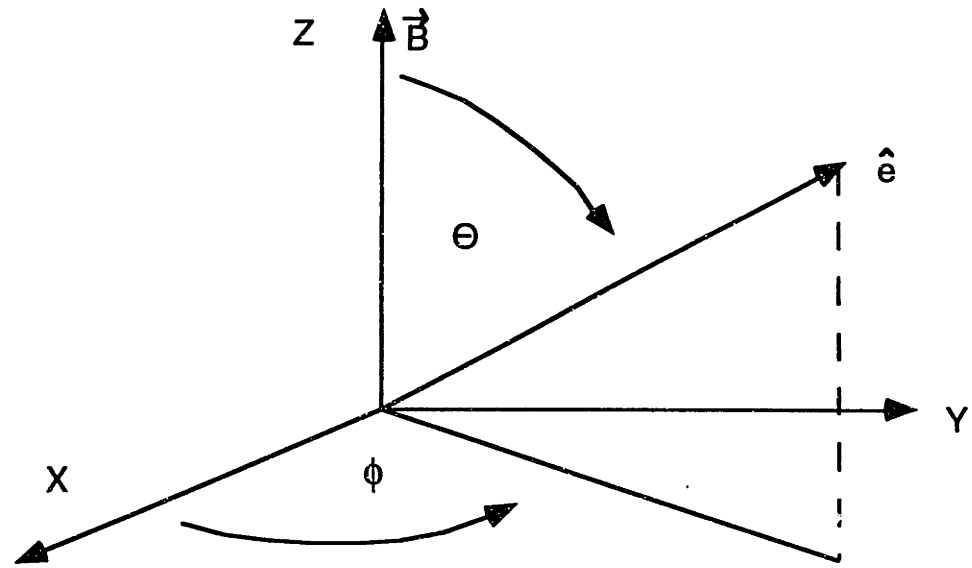

Figure 3.4 The relative orientation of the local magnetic field and the polarization vector of the rf.

$$H = \omega_0 F_z + \omega a^+ a + \lambda\left[\left(\hat{e}\cdot\vec{F}\right)a + \left(\hat{e}^*\cdot\vec{F}\right)a^+\right].$$

Using the basis vectors

$$\hat{e}_+ = \frac{1}{\sqrt{2}}\left(\hat{e}_x + i\hat{e}_y\right)$$

$$\hat{e}_- = \frac{1}{\sqrt{2}}\left(\hat{e}_x - i\hat{e}_y\right)$$

and angular momentum operators

$$F_+ = \frac{1}{\sqrt{2}}\left(F_x + iF_y\right)$$

$$F_- = \frac{1}{\sqrt{2}}\left(F_x - iF_y\right)$$

the Hamiltonian can be written in the form

$$H = \omega_0 F_z + \omega a^+ a + \lambda\left\{F_z\left(a + a^+\right) + \frac{1}{\sqrt{2}}\sin\theta\left[e^{-i\phi}\left(F_+ a + F_- a^+\right) + e^{i\phi}\left(F_- a + F_+ a^+\right)\right]\right\}.$$

In applying this Hamiltonian to the system we will ignore transitions which are far from resonance (we are therefore neglecting the Bloch-Siegert shift). The total angular momentum of the atom plus photon system is conserved; the z component is $m_F + N$ where N is the total number of photons in the field. In a three level atomic system there are three basis vectors with eigenvalue N of the z component of the total angular momentum:

$|+,N-1\rangle$

$|0,N\rangle$.

$|-,N+1\rangle$

The eigenenergies γ of this Hamiltonian are determined from the equation

$$\det(H-I\gamma)=\det\begin{pmatrix}(\omega_0+(N-1)\omega)-\gamma & \omega_R\frac{\sin\theta}{2}e^{-i\phi} & 0\\ \omega_R\frac{\sin\theta}{2}e^{i\phi} & (N\omega)-\gamma & 0\\ 0 & 0 & (-\omega_0+(N-1)\omega)-\gamma\end{pmatrix}=0$$

The Rabi frequency ω_R is defined as

$\omega_R=\sqrt{2}\lambda\sqrt{N}$.

$\omega_R{}^2$ is proportional to the number of photons per unit volume and is therefore proportional to the applied intensity of the rf field. Defining $\delta=\omega-\omega_0$, results in the following solutions

$\gamma=N\omega$

$$\gamma=N\omega\pm\sqrt{\delta^2+\frac{\omega_R{}^2}{4}\sin^2\theta}$$

and we refer to the eigenstates with these eigenenergies as

$|N,0\rangle$

$|N,+\rangle$

$|N,-\rangle$

If we look at these solutions in the plane where theta equals zero we see that if an atom in the $|N,-\rangle$ state travels outward from the origin it will interact with the rf field when delta equals zero (see fig. 3.5). At this point it will undergo stimulated emission of two photons and will then be expelled from the trap. This is the basic mechanism for evaporation.

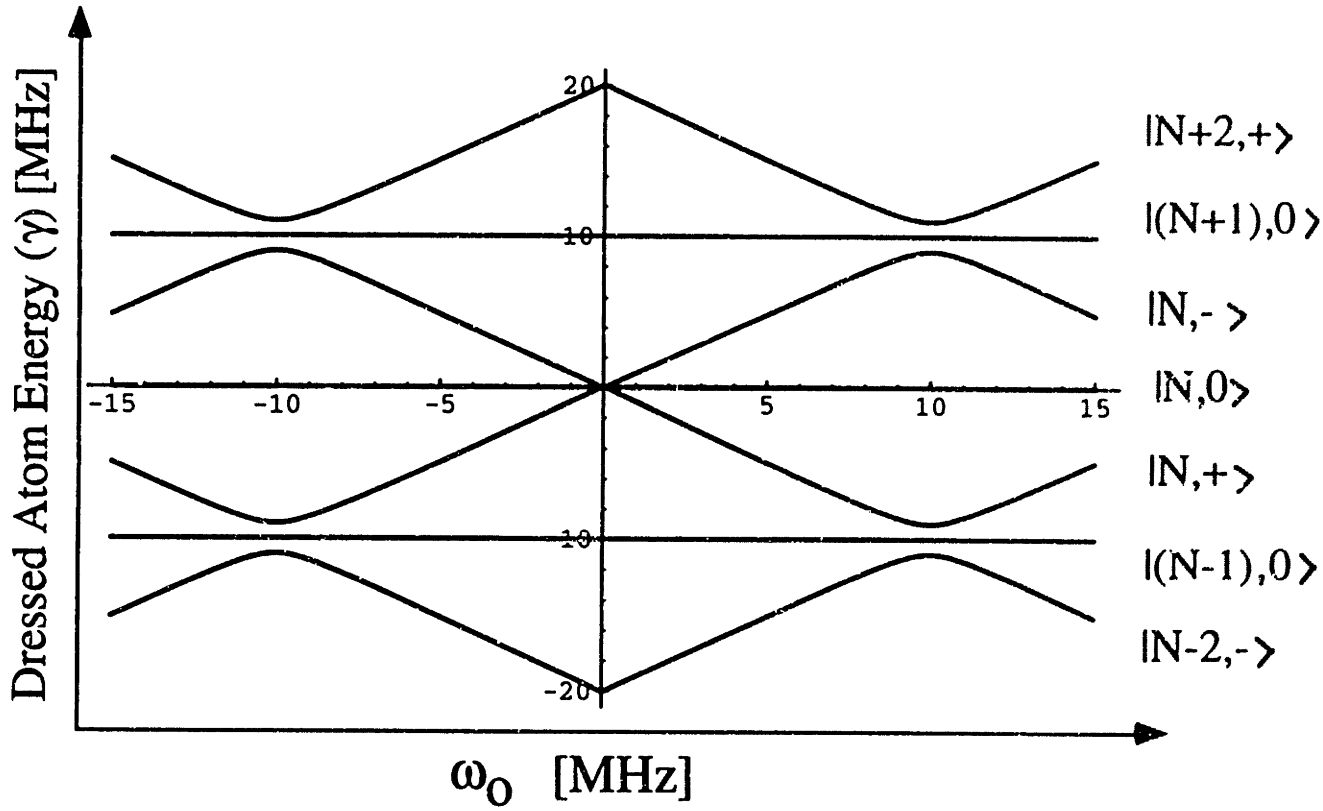

Figure 3.5 Dressed atom eigenstate energies versus magnetic field

Another interesting result that can be explored is how the rf interacts with the atom as a function of position inside the trap. The interaction of the rf with the atom (characterized by the Rabi frequency) is proportional to the dot product of the atom's magnetic moment with the polarization vector of the rf field. The angular dependence of the Rabi frequency as is shown in figure. 3.6. Evaporation occurs on a ellipsoidal equipotential surface defined by the resonance condition $\mu|B|= h\nu_{rf}$. The Rabi frequency on this surface varies as $\sin\theta$, therefore along the polarization direction of the rf virtually no atoms are evaporated.

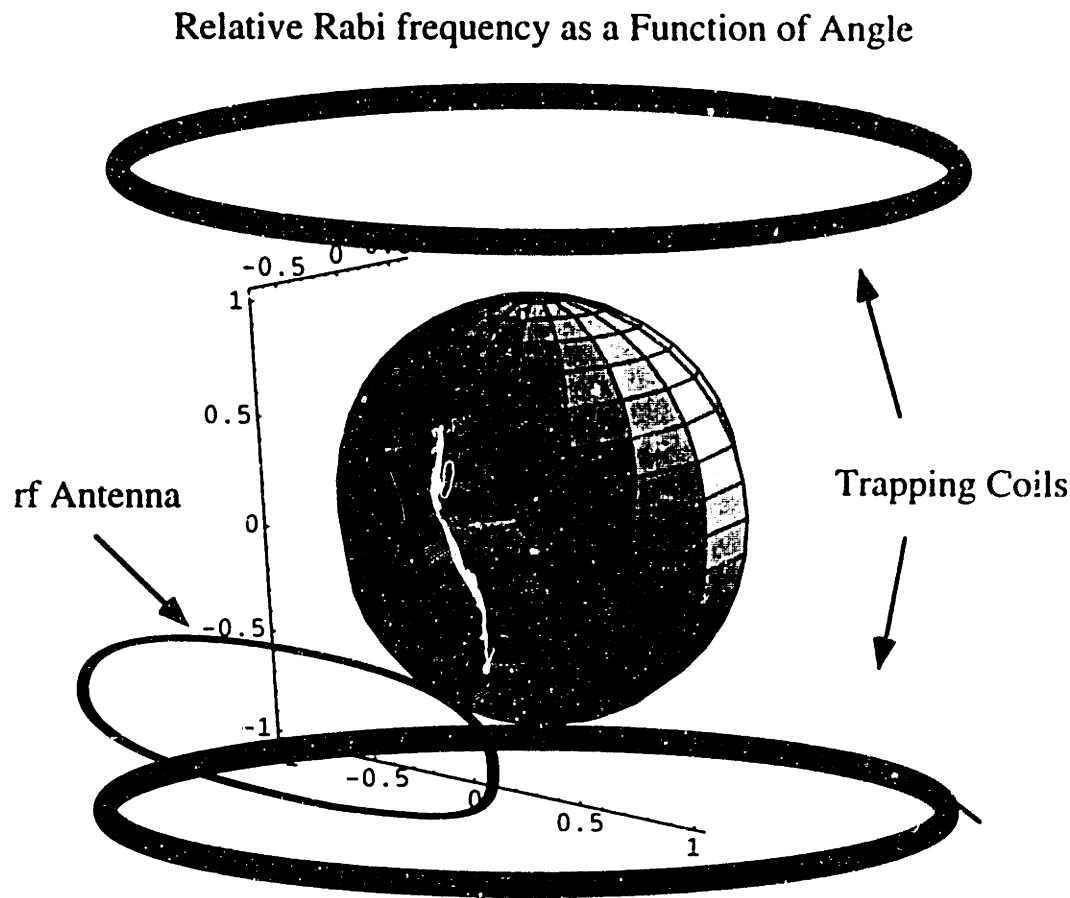

Figure 3.6 The Rabi frequency is proportional to the radius as a function of angle in the above diagram. The rf intensity seen by the atom is proportional to $|\mathbf{B}\times\mathbf{e}|^2$ where **B** is the local magnetic field, and **e** is the polarization of the radiation. The Rabi frequency is weakest along the symmetry axis of the rf antenna.

It is important to determine the magnitude of the AC magnetic field required to evaporate atoms. We consider the field sufficient for evaporation if the probability of an atom being spin flipped is 50% when the atom passes through the resonance. The transition probability occurring is given by the Landau-Zener formula[25]

$$P = 1 - e^{-2\pi\frac{\hbar\omega_R^2}{(dE/dt)}}.$$

ω_R is the Rabi frequency of the rf and dE/dt is the time rate of change of the atom's energy.

For an atom, with a magnetic moment μ, moving, with velocity v, in an inhomogeneous magnetic field, with gradient B', dE/dt is given by

$$\frac{dE}{dt} = \mu\frac{dB}{dx}\frac{dx}{dt} = \mu B' v.$$

The Rabi frequency for a 50% transition probability obeys the following equation

$$\omega_R^2 = \frac{\ln(2)\mu B' v}{h}.$$

For typical experimental parameters this implies a Rabi frequency of 120 kHz, corresponding to an AC magnetic field amplitude B_{AC} of approximately 260 mG. B_{AC} and the Rabi frequency are related by

$$\mu B_{AC} / \sqrt{2} = \hbar \omega_R.$$

3.4 Experimental Results

As a result of our careful preparation we were able to obtain samples of magnetically trapped atoms with densities of 5 x 10^{11} cm^{-3} and temperatures of 1 mK. At this combination of density and temperature, the elastic collision rate was 20 Hz (per atom in the trap). This rate was high in comparison to our loss rate, due to background gas collisions, which was about 0.03 Hz. Given that we also had the ability to remove the highest energy atoms from the sample via rf spin flips we were in an excellent position to observe evaporative cooling.

We were able to evaporatively cool our sample of atoms increasing the phase space density by a factor of 190. This was done in such a way that the elastic collision rate was increasing as we cooled, resulting in self accelerating evaporation. In addition the elastic collision cross section for cold sodium atoms was determined to be 6 10^{-12} cm^{-3}. Non adiabatic spin flips at the trap center were identified as the major obstacle to further cooling. A description of this experiment can be found in the paper "Evaporative Cooling of Sodium Atoms" in the appendix to Chapter 3.

There are a few points regarding the detection and analysis not contained in this paper which I would like to expand upon in more detail. The absorption images were taken with a very weak probe intensity, typically 10 nW and a probe pulse duration of 1 ms. Therefore each pulse contained about 3 x 10^7 photons compared to more than 10^9 atoms in

the trap. Our absorption images were non-destructive, and allowed us to take several pictures of the same cloud.

Detecting such a small number of photons required a sensitive detector. The absorption beam was imaged onto a Princeton Instruments CCD camera (model number TE/CCD-576). This camera has a pixel array containing about 150,000 pixels. For a typical probe pulse we get about 200 photons per pixel. The quantum efficiency of this detector is 50% resulting, after some image processing in, a signal to noise ration of 10 to 1.

Deriving temperatures and densities from an absorption image is in principle straight forward. In a conservative potential such as our magnetic trap the width of the image is proportional to the temperature. The transmitted light intensity is proportional to Exp[-$\int n(x)\sigma(x)dx$] where n(x) is the density as a function of position along the propagation direction of the probe light and $\sigma(x)$ is the light absorption cross section. If $\sigma(x)$ is constant, the logarithm of the transmitted light intensity is proportional to the column density ($\int n(x)dx$) of the atoms. Unfortunately there are a number of effects which complicate this simple interpretation of the absorption images.

Some atoms inside the magnetic trap, before evaporation, were sampling magnetic fields on the order of 100 Gauss. Thus light which is off resonant for atoms at the center of the trap might be right on resonance for atoms displaced from the origin.

There is also the additional complexity that both the atoms and the light are polarized, but the atoms polarization direction is a function of position inside the trap. Therefore there are transitions which are dipole forbidden in one part of the cloud and allowed in other parts. The Zeeman shifts and the changing orientation of the atoms make $\sigma(x)$ strongly position dependent. Furthermore the atomic cloud is an optically active medium, rotating the polarization of the probe beam as it passes through the cloud. All of these effects are accounted for and simulated in a computer program written by a member of our group, and will be discussed in detail in his thesis [26].

Appendix to Chapter 3

In the following appendix two papers are presented. The first "An analytic model for evaporative cooling of atoms" has been published in *Applied Physics B* (Volume 60 pages 155-159, 1995). The second paper "Evaporative Cooling of Sodium Atoms" has been accepted for publication in *Physical Review Letters.*

An analytical model for evaporative cooling of atoms

Kendall B. Davis, Marc-Oliver Mewes, and Wolfgang Ketterle

Department of Physics and Research Laboratory of Electronics

Massachusetts Institute of Technology, Cambridge, MA 02139

Tel. (617) 253-6815, FAX (617) 253-4876, E-Mail: WOLFGANG@AMO.MIT.EDU

Abstract

Evaporative cooling of trapped atoms is described as a sequence of truncation of the high energy tail of the thermal distribution followed by collisional relaxation. This model is solved analytically for arbitrary power-law potentials. The threshold density for accelerated evaporation is found to be lowest in a three-dimensional linear potential.

PACS: 32.80.Ps, 42.50.Vk

Introduction

Although laser cooling has seen rapid progress in the last few years it still has several severe limitations. There are absorption effects [1, 2] limiting the density of cold atoms, the recoil limit, also heating and trap loss due to excited state collisions. All of these limitations do not apply to evaporative cooling. In addition, atoms such as hydrogen which don't have convenient optical transitions can be evaporatively cooled. Until recently, evaporative cooling could only be applied to atomic hydrogen which can be pre-cooled by cryogenic methods [3-6]. Several groups are currently trying to extend evaporative cooling to laser cooled atoms, and very recently two successful demonstrations were reported [7, 8].

Evaporative cooling was originally proposed by Hess [9]. It consists of the selective removal of atoms in the high energy tail of the thermal distribution and the collisional equilibration of the remaining atoms. Although neither the selection of atoms nor collisions alone increase the phase space density, the combination of both does [10]. It is even possible to simultaneously obtain a decrease in temperature and an increase in density if the shrinking volume of the atom cloud overcompensates for the loss in the number.

With reference to magnetically trapped hydrogen, several theoretical studies of evaporative cooling have been reported [11-15]. Some of these models included not only evaporative loss of atoms, but also dipolar relaxation [12-14] and three-body recombination [13, 14]. Presented here is a simplified analytical description including only elastic collisions, evaporative loss of particles and background gas collisions. One motivation for such a simple model is the fact that for alkali atoms the elastic cross section is roughly three orders of magnitude larger than for hydrogen. As a result, inelastic processes are negligible for a broad regime of temperature and density which is of interest for several experiments [7, 8]. A different analytical model for evaporation is discussed in Ref. [15] and could probably be applied to the situation discussed here.

The most important parameter to control the evaporation is the depth η kT of the potential well. For small η, a large fraction of the atoms can escape over the threshold of the potential resulting in fast evaporation; however, the temperature reduction per escaping atom is small. It is this interplay between the truncation parameter η and the dynamics of the evaporation which is described in our model. In the most general situation η will be varied with time to control and optimize the evaporation process. In this paper, we mainly study the effects of a single truncation step as a function of η.

Experiments on evaporation employ linear [7, 8] and harmonic [16] traps; the hydrogen work at MIT uses an anisotropic trap which can be regarded as a two-dimensional linear potential with steep walls providing confinement in the third dimension [3, 13]. The model presented here is valid for any number of dimensions and arbitrary power law potentials. One rather unexpected result is that the important self-acceleration of evaporation is only pronounced in linear potentials.

The basic model

We model evaporative cooling as a discrete process. Truncation of the energy distribution at η kT is followed by thermal relaxation in an infinitely deep potential resulting in a temperature decrease from the initial temperature T to T'. This cycle is repeated with an energy truncation at η kT' etc. In most experiments, the potential depth is lowered continuously while the atoms stay in thermal equilibrium through elastic collisions. The discrete model has the advantage of having an exact solution and can be used to study the basic interplay between the various parameters of the evaporation process.

During one cycle, the number of trapped atoms is reduced from N to N'. It is convenient to express all important quantities as power laws ν^x with $\nu = N'/N$. Defining

$$\gamma = \frac{\log(T'/T)}{\log(N'/N)} \tag{1}$$

the temperature changes as $T'/T = \nu^\gamma$ during one cycle.

In a d-dimensional potential

$$U(r) = \text{const. } r^m, \tag{2}$$

the volume occupied by the trapped atoms scales as $T^{d/m}$. This scaling arguments it independent on how the volume is defined (e.g. by a 1/e decay of the density, or as the number of atoms divided by peak density). Note that the potential in a spherical quadrupole magnetic trap is anisotropic, but it can be written in the form of equation (1) after a coordinate transformation $z' = 2\,z$.

For the density n, one obtains a power law

$$n'/n = \nu^{1-\xi\gamma} \tag{3}$$

with

$\xi = d/m.$

Since we are only interested in ratios n'/n, (3) holds for the peak density as well as the average density. Power laws exist for all other quantities (Table 1).

If j discrete evaporation steps are performed, ν has to be substituted by ν^j. The dynamics of evaporation is entirely described by the two quantities ν and γ.

These two quantities are calculated for an arbitrary power law potential r^m in d dimensions from integrals involving the density of states D(E)

$$D(E) = \frac{(2M)^{3/2}}{\hbar^3\,(2\pi)^2} \int_{V(E)} \sqrt{E - \text{const. } r^m}\; d^3r. \tag{4}$$

V(E) is the available position space for particles with energy E and atomic mass M [17]. Note that we are always considering a three-dimensional gas confined in d dimensions (either unconfined in the remaining 3-d dimensions or confined by infinitely steep walls).

The occupation number of classical particles in an energy level E in the trap is $\exp(-(E-\mu)/kT)$. Effects of quantum statistics can be neglected for a dilute gas. The fraction ν of particles with energy E smaller than $\eta\,kT$ is

$$\nu(\eta) = \frac{1}{N}\int_0^{\eta kT} D(E)\, e^{-(E-\mu)/kT}\, dE\ .$$

The chemical potential μ is determined by the normalization $\nu(\infty) = N$.

Introducing the normalized energy $\varepsilon = E/kT$ and $\sigma(\varepsilon) = (kT/N)\, D(\varepsilon\, kT)\, e^{\mu/kT}$ as the normalized density of states one obtains

$$\nu(\eta) = \int_0^{\eta} \sigma(\varepsilon)\, e^{-\varepsilon}\, d\varepsilon \tag{5}$$

with

$$\sigma(\varepsilon) = \frac{\varepsilon^{1/2+\xi}}{\Gamma(3/2 + \xi)}\ . \tag{6}$$

Note that the chemical potential and the constants in (4) are both absorbed in the normalization factor in (6). The integral in Eq. (5) can be solved in terms of generalized Gamma functions which are reduced for specific values of ξ to the expressions shown in Table 2.

The function $\gamma(\eta)$ is obtained from the total energy $\alpha(\eta)$ N kT of the trapped atoms after truncation

$$\alpha(\eta) = \int_0^{\eta} \varepsilon\, \sigma(\varepsilon)\, e^{-\varepsilon}\, d\varepsilon. \tag{7}$$

The average total energy per atom in units of kT is $\alpha(\eta)/\nu(\eta)$.

For $\eta \rightarrow \infty$, one obtains

$$\alpha(\infty) = (3/2) + \xi. \tag{8}$$

$\alpha(\eta)$ can be obtained in analytical form (Table 2). The normalized energy per atom after rethermalization gives the decrease in temperature from T to T' per evaporation cycle

$$\frac{T'}{T} = \frac{\alpha(\eta)}{\nu(\eta)\,\alpha(\infty)} .$$

From Eq. (1) one obtains

$$\gamma = \frac{\log\left[\dfrac{\alpha(\eta)}{\nu(\eta)\,\alpha(\infty)}\right]}{\log(\nu(\eta))} . \tag{9}$$

The average energy of an evaporated atom is ε_{eff} kT with

$$\varepsilon_{eff} = \frac{\alpha(\infty)-\alpha(\eta)}{1-\nu(\eta)} , \tag{10 a}$$

or equivalently,

$$\varepsilon_{eff} = \left[\xi+\frac{3}{2}\right]\frac{1-\nu(\eta)^{\gamma(\eta)+1}}{1-\nu(\eta)} . \tag{10 b}$$

For a large cutoff parameter η, $\nu(\eta) \rightarrow 1$. Expanding Eq. (10 b) by treating $1-\nu(\eta)$ as a small parameter, yields

$$\gamma = \frac{\varepsilon_{eff}}{(3/2) + \xi} - 1 .$$

Therefore, for large η, γ is a dimensionless quantity characterizing how much more than the average energy is removed by the evaporated atoms. A similar equation was used by Hess (Eq. (4) in [9]) including magnetic decompression and losses due to dipolar relaxation. For large truncation parameters η, one can integrate (10 a) by parts and obtains $\varepsilon_{eff} \rightarrow \eta + 1$, implying $\gamma \rightarrow \infty$. The temperature reduction per evaporated atom is large, but the evaporation process is slow because there are only few atoms with energy larger than η kT.

For small η, one obtains from (5), (7) and (9) $\gamma = \dfrac{2}{3+2\xi}$. On first sight, it is surprising that the increase in phase-space density has its maximum for $\eta \rightarrow 0$ (see figure 2). However, this corresponds to the selection of the energy levels with the largest population.

After thermalization, the lowest levels have even larger population corresponding to an increase in phase-space density (see also Ref. [10]).

Comparison for different potentials

In the following discussion we examine evaporation in different trap geometries. Notice, that for this purpose, it is more natural to measure energies not in units of kT, but rather in units of the average total energy $(\frac{3}{2}+\xi)$ kT. We denote energies and truncation parameters normalized in this way by $\tilde{\varepsilon}$ and $\tilde{\eta}$ respectively, i.e.

$$\tilde{\varepsilon} = \frac{\varepsilon}{\frac{3}{2}+\xi} . \tag{11}$$

The normalized density of occupied states,

$$\tilde{p}(\tilde{\varepsilon}) = \sigma(\varepsilon)\ (\tfrac{3}{2}+\xi)\, e^{-\varepsilon} \tag{12}$$

(normalized in such a way that $\int_0^\infty \tilde{p}(\tilde{\varepsilon})\, d\tilde{\varepsilon} = 1$) is similar for different trap geometries having a peak centered around the average energy (normalized to 1) with a width of approximately 1 (Fig. 1). It is therefore not surprising, that the functions ν and γ are similar too, or in other words, the decrease in atom number and in temperature is similar for different potentials when the energy truncation is performed at the same $\tilde{\eta}$. This conclusion is not valid at very small or large $\tilde{\eta}$, but these regions are of minor practical interest for evaporative cooling.

In contrast, the density increase is much larger for large ξ since the volume of the trapped sample scales with temperature as T^{ξ}. Similarly, the changes in phase space density ρ and elastic collision rate strongly depend on the potential parameter ξ (Fig. 2). (The elastic collision rate is given by $n\sigma_{el}\, v$, where σ_{el} denotes the elastic collision cross section and v the atomic velocity.) In current experiments with laser cooled atoms, the initial density is just sufficient to start the evaporative cooling process because the thermalization time

(which is inversely proportional to the elastic collision rate) is comparable to the trapping time. Significant evaporative cooling probably requires a speed-up in the thermalization rate. This means that the cloud has to be truncated at sufficiently large η or γ. Indeed, from Table 1 one obtains the inequality

$$\gamma > \frac{1}{\xi - 1/2}$$

for accelerated collision rates. For larger potential parameters ξ, evaporation at smaller γ is favorable (Fig. 2). Indeed, for a three-dimensional linear potential (ξ=3), the largest increase in the thermalization rate is found at $\tilde{\eta} = 0.8$. At such values of $\tilde{\eta}$, a parabolic trap (ξ=3/2) would already exhibit a decrease of the thermalization rate. Evaporation at such small $\tilde{\eta}$ values is accompanied by a substantial loss of trapped particles. Experiments employing this strategy might eventually be limited by the sensitivity of probing very few atoms.

Inclusion of background gas collisions

So far, we have not taken into account loss of atoms due to background gas collisions. If the trapping time is t_{trap}, and one evaporation cycle is carried out in a time interval t_{step}, the number of particles is reduced by an additional factor $e^{(1/\tau)}$ during this cycle with

$$\tau = t_{trap}/t_{step}. \qquad (13)$$

We can incorporate this loss process by considering one evaporation cycle as consisting of three steps: truncation at η, rethermalization, loss of particles by a factor $e^{(1/\tau)}$. We could incorporate this additional loss in the number of atoms into the exponents in Table 1 as was done by Hess for the γ exponent [9]. However, an equivalent approach chosen here is to calculate all quantities without trap loss and then multiply N, n, ρ and nv by $e^{-(1/\tau)}$ and leave T and V unchanged.

Snoke and collaborators have shown that the energy distribution is almost indistinguishable from the equilibrium distribution after five collisions [18, 19]. τ is then approximately one fifth of the ratio between the elastic collision rate and the trap loss collision rate which is colloquially called the ratio of good to bad collisions.

In the absence of trap loss, the maximum increase in the thermalization rate is 1.04 for a parabolic potential and 1.59 for a three-dimensional linear potential (Fig. 2). This big difference is a consequence of the more pronounced shrinking of the cloud with temperature for large ξ which furthermore allows evaporation to be carried out at smaller truncation parameters $\tilde{\eta}$. Figure 3a and c show the increase in the thermalization rate for several values of τ. Accelerated evaporation requires a minimum value of τ which is 2.2 for the three-dimensional linear potential and 24 for the parabolic case, more than an order of magnitude higher. This means that accelerated evaporation in a parabolic trap requires considerably higher initial density or lower residual gas pressure than in a spherical quadrupole trap. However, a parabolic trap with a very small bias field (e.g. a Ioffe trap) has a linear potential in the two transverse directions except for a small region at the bottom which is rounded off. If the atom cloud extends well beyond the parabolic region, the trap can be regarded as a linear trap in two dimensions and a parabolic trap in the third dimension, corresponding to ξ= 5/2 (see Ref. [17] for the derivation of the density of states for traps with different power laws of the potential in different dimensions). Such a field configuration would avoid trap loss due to Majorana flops at the zero of the magnetic field, and simultaneously provide tight enough confinement for accelerated evaporation.

A more refined model should account for the change in the elastic collision rate during thermalization. Immediately after truncation the rate is smaller than before truncation by approximately a factor $\frac{N' v'}{Nv} = \nu^{1+\gamma/2}$. This reduction shifts the optimum strategy to larger values of $\tilde{\eta}$. In a worst case model, we assume that the elastic collision rate during a thermalization step is constant and equal to the rate immediately after truncation. The

number τ of truncation/thermalization steps during one trapping time is then dependent on $\tilde{\eta}$ through

$$\tau = \tau_0 \nu^{1+\gamma/2} \tag{14}$$

where τ_0 is inversely proportional to the thermalization time before truncation.

We find the minimum τ_0 for accelerated evaporation to be 4.7 for the spherical quadrupole trap and 29 for the parabolic trap. The latter value corresponds to roughly 150 elastic collisions per trapping time in agreement with the same value obtained in Ref. [16] from Monte-Carlo simulations. The threshold for accelerated evaporation in a spherical quadrupole trap should be as low as approximately 25 elastic collisions per atom and trapping time.

With Eq. (14), the optimum increase in phase-space density no longer happens for $\eta \rightarrow 0$. The long thermalization time after a deep truncation results in increased loss of atoms due to background gas collisions and favors truncation at larger η. Optimized strategies for multi-step evaporation require additional study. For instance, if the overall goal is to maximize phase-space density, it could be more advantageous to focus first on increased thermalization rate and then to maximize phase space density when fast thermalization times prevent excessive loss of atoms due to background gas collisions. However, one possible simple strategy is obvious without further elaboration: if the initial conditions for accelerated evaporation are met and η is kept in the range for increased collision rates, density and phase space density will continuously increase. Ultimately, this increase is limited by loss processes (dipolar relaxation and three-body recombination) which are neglected in the model discussed here.

Conclusions

In conclusion, we have presented a simple formalism to treat evaporative cooling of trapped atoms. This formalism provides guidance to optimize forced evaporation (i.e.

variation of the potential depth with time). Different strategies maximize the increase in density, phase space density or thermalization rate. An important prediction is that the threshold density for accelerated evaporation is considerably higher in a parabolic trap than in a spherical quadrupole trap.

Acknowledgments: It is a pleasure to dedicate this paper to H. Walther who introduced one of us (W.K.) to the excitement of atomic physics. This work was supported by the Office of Naval Research and Air Force Office of Scientific Research through grant N00014-90-J-1642, the Joint Services Electronics Program and the Sloan Foundation. M.-O.M. and K.B.D. would like to acknowledge support from Studienstiftung des Deutschen Volkes and the M.I.T. Physics Dept. Lester Wolfe fellowship, respectively.

References

1. D.W. Sesko, T.G. Walker, and C.E. Wieman, J. Opt. Soc. Am. B 8, 946 (1991).

2. W. Ketterle, K.B. Davis, M.A. Joffe, A. Martin, and D.E. Pritchard, Phys. Rev. Lett. 70, 2253 (1993).

3. N. Masuhara, J.M. Doyle, J.C. Sandberg, D. Kleppner, T.J. Greytak, H.F. Hess, and G.P. Kochanski, Phys. Rev. Lett. 61, 935 (1988).

4. J.M. Doyle, J.C. Sandberg, I.A. Yu, C.L. Cesar, D. Kleppner, and T.J. Greytak, Phys. Rev. Lett. 67, 603 (1991).

5. O.J. Luiten, H.G.C. Werij, I.D. Setija, M.W. Reynolds, T.W. Hijmans, and J.T.M. Walraven, Phys. Rev. Lett. 70, 544 (1993).

6. I.D. Setija, H.G.C. Werij, O.J. Luiten, M.W. Reynolds, T.W. Hijmans, and J.T.M. Walraven, Phys. Rev. Lett. 70, 2257 (1993).

7. W. Petrich, M.H. Anderson, J.R. Ensher, and E.A. Cornell, in Fourteenth International Conference on Atomic Physics, Boulder, Colorado, 1994, Book of Abstracts, 1M-7.

8. K.B. Davis, M.O. Mewes, M.A. Joffe, and W. Ketterle, in Fourteenth International Conference on Atomic Physics, Boulder, Colorado, 1994, Book of Abstracts, 1-M3.

9. H.F. Hess, Phys. Rev. B 34, 3476 (1986).

10. W. Ketterle and D.E. Pritchard, Phys. Rev. A 46, 4051 (1992).

11. R.V.E. Lovelace, C. Mahanian, T.J. Tommila, and D.M. Lee, Nature 318, 30 (1985).

12. T. Tommila, Europhys. Lett. 2, 789 (1986).

13. J.M. Doyle. Ph.D. Thesis, Massachusetts Institute of Technology, 1991.

14. J.M. Doyle, J.C. Sandberg, I.A. Yu, C.L. Cesar, D. Kleppner, and T.J. Greytag, Physica B 194-196, 13 (1994).

15. O.J. Luiten. Ph.D. Thesis, University of Amsterdam, 1993.

16. C.R. Monroe, E.A. Cornell, C.A. Sackett, C.J. Myatt, and C.E. Wieman, Phys. Rev. Lett. 70, 414 (1993).

17. V. Bagnato, D.E. Pritchard, and D. Kleppner, Phys. Rev. A 35, 4354 (1987).

18. D.W. Snoke and J.P. Wolfe, Phys. Rev. B 39, 4030 (1989).

19. D.W. Snoke, W.W. Rühle, Y.-C. Lu, and E. Bauser, Phys. Rev. B 45, 10979 (1992).

Tables

Table 1

During evaporative cooling, all relevant quantities scale as ν^x where ν is proportional to the number of trapped particles.

Quantity	Exponent x
Number of atoms N	1
Temperature T	γ
Volume V	$\xi\gamma$
Density n	$1 - \xi\gamma$
Phase space density γ	$1 - \gamma(\xi + 3/2)$
Elastic collision rate n v	$1 - \gamma(\xi - 1/2)$

Table 2

The evaporation process in a d-dimensional potential r^m is described by two characteristic functions $\alpha(\eta)$ and $\nu(\eta)$ which depend only on $\xi = d/m$.

ξ	$\nu(\eta)$	$\alpha(\eta)$
3/2	$1 - \frac{2 + 2\eta + \eta^2}{2 e^{\eta}}$	$3 - \frac{6 + 6\eta + 3\eta^2 + \eta^3}{2 e^{\eta}}$
2	$\frac{-2\sqrt{\eta}\,(15+10\eta+4\eta^2)}{15 e^{\eta}\sqrt{\Pi}} + \mathrm{erf}[\sqrt{\eta}]$	$\frac{-\sqrt{\eta}\,(105+70\eta+28\eta^2+8\eta^3)}{15 e^{\eta}\sqrt{\Pi}} + \frac{7\,\mathrm{erf}[\sqrt{\eta}]}{2}$
3	$\frac{-2\sqrt{\eta}\,(105+70\eta+28\eta^2+8\eta^3)}{105 e^{\eta}\sqrt{\Pi}} + \mathrm{erf}[\sqrt{\eta}]$	$\frac{-\sqrt{\eta}\,(945+630\eta+252\eta^2+72\eta^3+16\eta^4)}{105 e^{\eta}\sqrt{\Pi}} + \frac{9\,\mathrm{erf}[\sqrt{\eta}]}{2}$

Figure Captions

Figure 1

Population of energy levels $\tilde{p}(\tilde{\varepsilon})$ (Eq. (12)). The dotted, dashed and solid curves are for $\xi = 3/2$ (3-dim. harmonic potential), $\xi = 2$ (2-dim. linear potential), $\xi = 3$ (3-dim. linear potential).

Figure 2

Dependence of various quantities during evaporation on the truncation parameter $\tilde{\eta}$. The dotted, dashed and solid curves are for $\xi = 3/2$ (3-dim. harmonic potential), $\xi = 2$ (2-dim. linear potential), $\xi = 3$ (3-dim. linear potential). The first graph shows the temperature exponent γ, the others the ratio of various quantities after and before a single truncation/thermalization step.

Figure 3

Relative change in the elastic collision rate versus truncation parameter $\tilde{\eta}$.

(a) 3-dim. linear potential ($\xi = 3$), the different trapping times are characterized by the values of τ (see (13)) given in the figure.

(b) same as (a), but using τ_0 as parameter (see Eq. (14)).

(c) same as (a), but for a 3-dim. harmonic potential ($\xi = 3/2$).

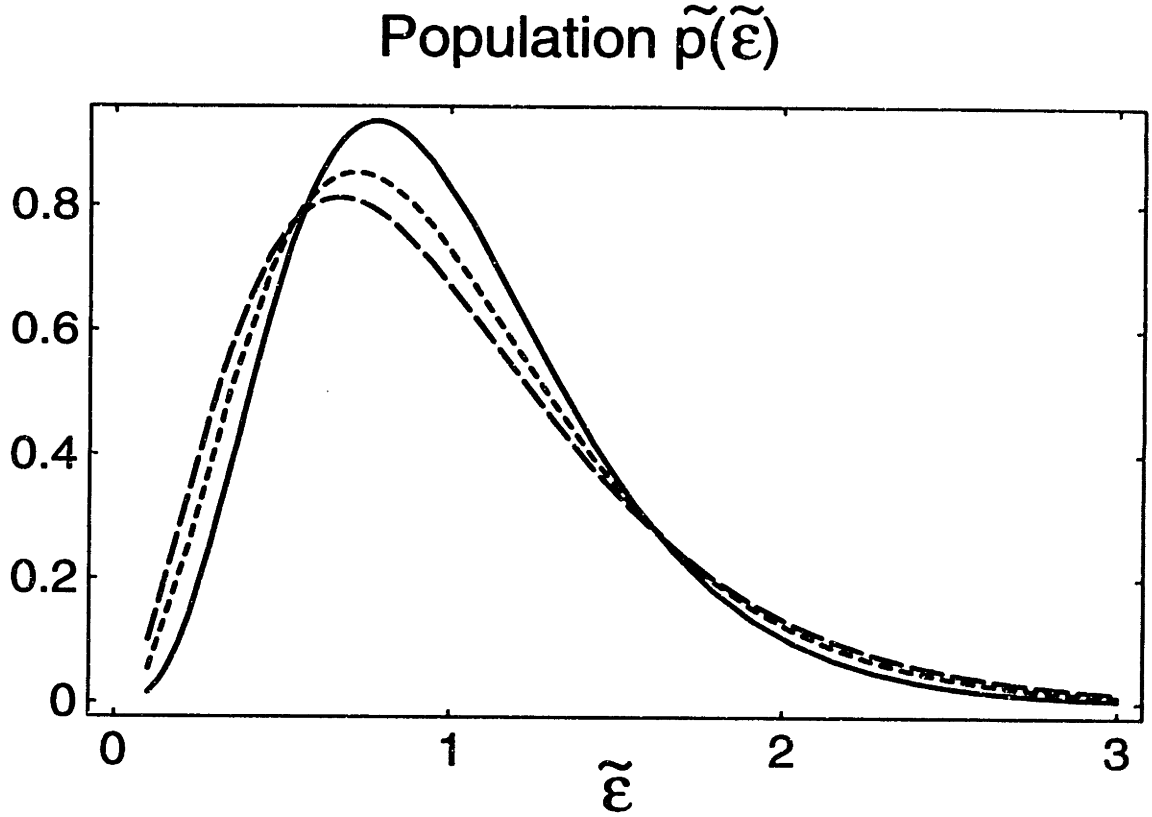
Population $\tilde{p}(\tilde{\varepsilon})$
0.8
0.6
0.4
0.2
0
0
1
2
3
$\tilde{\varepsilon}$

Figure 1

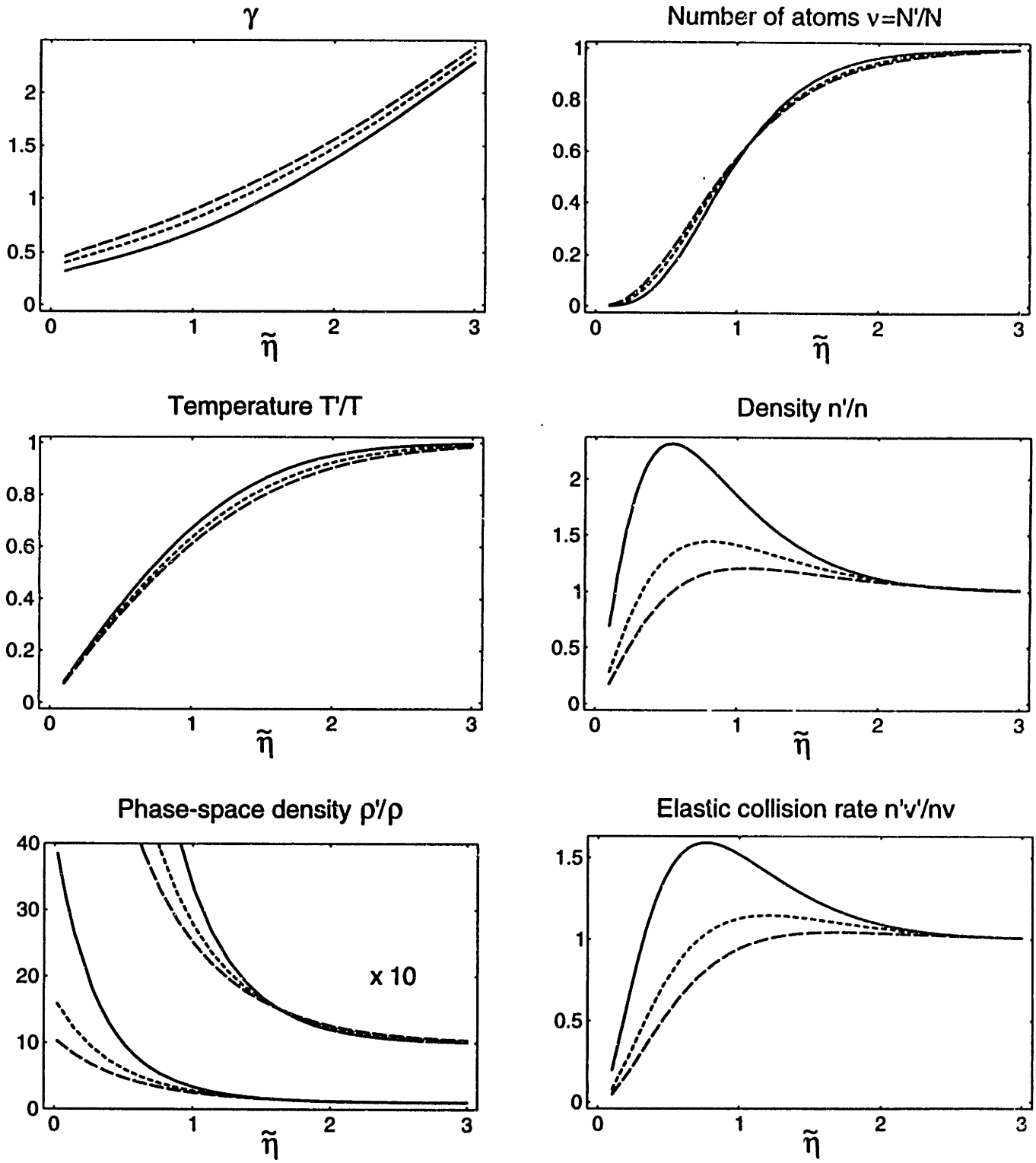
γ
Number of atoms ν=N'/N
Temperature T'/T
Density n'/n
Phase-space density ρ'/ρ
x 10
Elastic collision rate n'ν'/nν
η̃

Figure 2

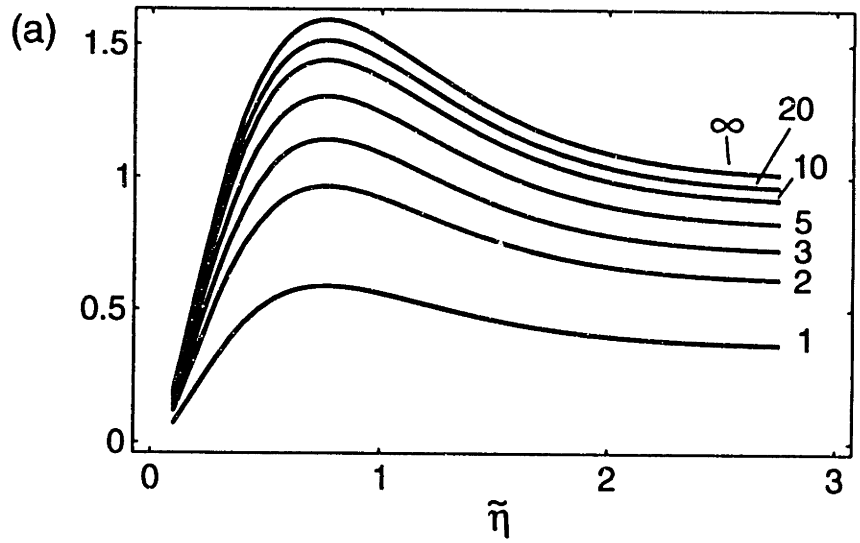
(a)
1.5
1
0.5
0
0
1
2
3
η̃
∞
20
10
5
3
2
1

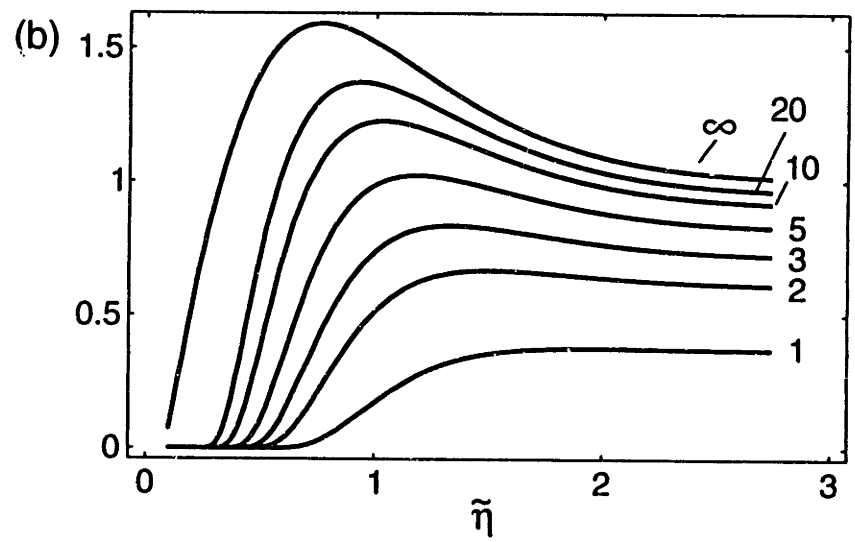
(b)
1.5
1
0.5
0
0
1
2
3
η̃
∞
20
10
5
3
2
1

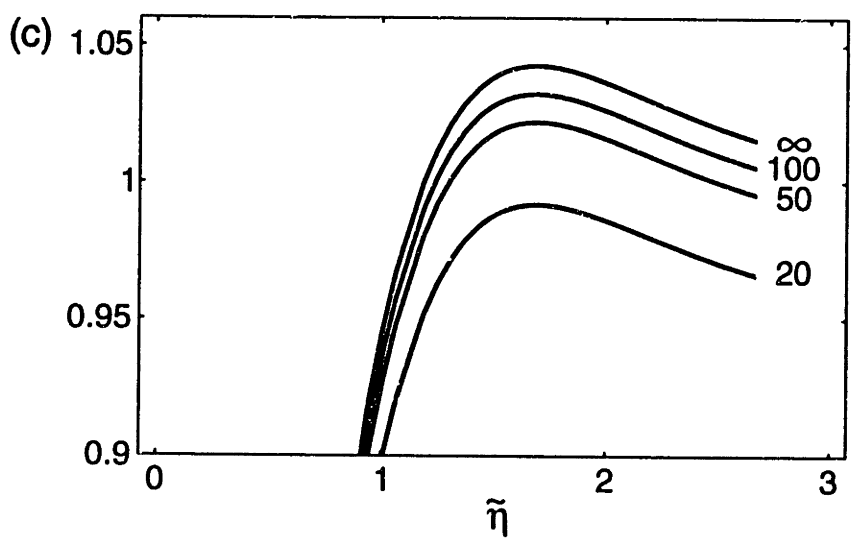
(c)
1.05
1
0.95
0.9
0
1
2
3
η̃
∞
100
50
20

Figure 3

Evaporative Cooling of Sodium Atoms

Kendall B. Davis, Marc-Oliver Mewes, Michael A. Joffe, Michael R. Andrews,

and Wolfgang Ketterle

Department of Physics and Research Laboratory of Electronics

Massachusetts Institute of Technology, Cambridge, MA 02139

Abstract

We have observed evaporative cooling of magnetically trapped sodium atoms. A novel technique, rf induced evaporation, was used to reduce the temperature by a factor of twelve and increase the phase space density by more than two orders of magnitude. The elastic collision cross section of cold sodium atoms in the F=1, m_F=-1 hyperfine state was determined to be 6 10^{-12} cm^2 which implies a positive value of the scattering length.

PACS: 32.80.Ps, 42.50.Vk

Cooling neutral atoms to sub-microkelvin temperatures offers the exciting possibility of studying novel phenomena at long deBroglie wavelengths, most notably quantum degeneracy effects. Furthermore, such cold atoms are promising for a host of scientific applications such as precision measurements, high resolution atom lithography and atom interferometry. Recently, several techniques have been demonstrated which allow cooling of atoms to temperatures below the recoil limit. Optical techniques such as Velocity Selective Coherent Population Trapping [1] and Raman cooling [2] have achieved sub-recoil temperatures in one or two dimensions. They work best at low atomic densities. At high densities, temperature and density are eventually limited by the absorption of incident or scattered light [3, 4] and by heating and trap loss due to excited state collisions [5]. The technique of forced evaporative cooling relies on collisional thermalization and has no recoil limit to overcome; therefore it seems ideally suited to reaching very low temperatures in dense atomic samples. Unfortunately, it requires high initial densities which could until recently only be prepared by cryogenic methods applicable solely to atomic hydrogen [6, 7].

In this paper we elaborate on our initial demonstration of evaporative cooling for an atom different from hydrogen, Na [8], that was contemporaneous with the announcement of similar results in Rb [9]. Very recently, evaporative cooling of Na has also been observed in an optical trap [10]. By using a combination of different cooling and trapping techniques involving lasers and magnetic fields we were able to obtain the high initial density required for evaporative cooling. This closes the gap between optical cooling at relatively low density and collisional cooling which requires high density, and frees evaporative cooling from the restrictions of a cryogenic environment by using laser cooling as the precooling stage. Furthermore, it has been pointed out that alkali atoms have advantages for evaporative cooling due to the large elastic cross section [11].

Evaporative cooling requires the selective removal of the most energetic atoms from the trap. When the remaining atoms rethermalize there is a net cooling effect [12]. The selection of evaporating atoms is usually done by lowering the height of the trapping potential [6].

Using this scheme in a spherical quadrupole trap would weaken the confinement, thus lower the density and slow down the evaporation process. This can be avoided in more complicated trapping geometries [6], but the spherical quadrupole trap provides the tightest confinement and has therefore advantages for evaporative cooling [13]. In this paper, we demonstrate a novel evaporation technique, rf induced evaporation, which was originally suggested in Ref. [14]. Atoms are removed from the trap by inducing an rf transition to an untrapped state without varying the trapping potential. Using this technique we observed strong evaporation of magnetically trapped sodium atoms lowering the temperature by a factor of twelve and increasing the phase space density by a factor of more than one hundred.

A high density of magnetically trapped atoms is obtained in a multistep procedure. Atoms were initially slowed in a Zeeman slower and loaded into a Dark SPOT [3]. Typically, 10^9 to 10^{10} atoms were confined at densities of $5\ 10^{11}$ cm^{-3}. Sub-Doppler temperatures of 100 μK were achieved by turning off the weak quadrupole magnetic field and applying a dark version of polarization gradient cooling. By employing very weak repumping sidebands, the density of atoms in the F=2 state is kept low enough to avoid absorption of the cooling light. This method should avoid heating effects due to high optical density as observed in Cs [15]. The laser light was quickly (< 1 ms) shut off and a magnetic quadrupole field of 100 G/cm switched on. Care was taken to provide a magnetic potential which is neither too steep (which would add too much potential energy causing heating), nor too shallow (which would result in a loss of density as the cloud expands). The density in the magnetic trap is a factor of ten lower than in the light trap because only about one third of the atoms are in the trapped F=1, $m_F = -1$ state, and because of some expansion of the cloud. Subsequently, the magnetic field gradient was increased to 1000 G/cm.

Adiabatic increase of a linear potential by a factor of η results in an increase in density by a factor of η and in temperature by a factor of $\eta^{2/3}$. The adiabaticity of the compression

was verified by expanding the cloud again and retrieving the initial temperature to within 10 %. The adiabatic increase of the field gradient by a factor of ten led to an enhancement of the elastic collision rate by a factor of twenty which was crucial for obtaining fast evaporation. The sample of atoms prepared in this way had typically 8 10^8 atoms at a peak density of 5 10^{11} and a temperature of 1 mK.

The number, density, temperature, and also the spatial distribution of the trapped atoms were determined by absorption imaging. Identical results obtained with two successive images of the same atoms verified that the probing was non-perturbative. Indeed, the number of absorbed photons was much less than one per atom. Atoms in our spherical quadrupole trap oscillate with an effective frequency on the order of kHz. This makes it rather difficult to suddenly switch off the magnetic trap and image the atoms at zero magnetic field. Therefore, the absorption images were taken in situ inside the magnetic trap and were compared to simulations that included the full hyperfine Hamiltonian and the varying magnetic field direction with respect to the probe polarization [16]. If the probe frequency is in resonance with a Zeeman shifted hyperfine transition in the spatial wings of the cloud, the absorption image appears wider. However, identical temperatures and densitites were obtained from the fits to images taken with different probe frequencies.

The major goal of this multi-step procedure of cooling and compressing atoms was to obtain a sample of magnetically trapped atoms with an elastic collision rate much higher than the loss rate due to background gas collisions. A residual gas pressure of about 5 10^{-11} mbar resulted in a trapping time of 30 s. In previous work [17] the time between collisions and the trapping time were both approximately 15 s. For our highest density samples, the average time between collisions was 20 ms (see below) resulting in 1500 collisions per trapping time, more than sufficient to study elastic collisions and observe evaporative cooling.

The driving process for evaporative cooling is elastic collisions. For sub-millikelvin sodium atoms only one or two partial waves (s- and d-wave) contribute to the scattering. Depending on the s-wave scattering phase shift, the zero-temperature cross section varies between zero and infinity. The phase shift depends critically on the binding energy of the last bound vibrational level and is very sensitive to fine details of the interaction potential.

We were able to deduce the elastic collision cross section by observing the thermalization of an atom cloud. For this, a non-thermal distribution was prepared by temporarily displacing the trap center by about 1 mm along the symmetry axis (z-axis). This was accomplished by suddenly imbalancing the current through the two solenoids of the spherical quadrupole trap. Within 100 ms, anharmonicities lead to dephasing of the initial oscillations, resulting in a cloud which was elongated along the z-direction. Using absorption imaging, the relaxation of this anisotropic energy distribution was observed by recording the shape of the cloud as a function of time [17]. In principle, equilibration might happen due to the ergodic evolution of orbits in the trap independent of collisions. However, Monte-Carlo simulations showed that the spherical quadrupole trap is non-ergodic for periods of at least 10 s. In addition, we lowered the density by a factor of twelve by optically pumping atoms to non-trapped states using off-resonant laser light, and found the 1/e relaxation time τ to be inversely proportional to the product of peak density n_0 times velocity (Fig. 1). From that we estimate a lower bound for the ergodic mixing time of 30 s, completely negligible to the observed relaxation time of 1 s. Note that we determined relaxation times for the uncompressed cloud. Assuming constant elastic cross section, adiabatic compression to the maximum field gradient reduces the relaxation time to about 50 ms, comparable to the dephasing time.

According to calculations by Snoke and Wolfe it takes five elastic collisions for complete thermalization [18]. Monte-Carlo calculations gave 2.7 for the ratio of elastic collision rate to the relaxation rate $1/\tau$ which describes the cross-sectional relaxation of a cloud with an anisotropic energy distribution[17].

We determine the elastic cross section σ from the equation $n_{eff}\,\sigma\,v = 2.7/\tau$, where $v = 4\,(k_B T/\pi\, m)^{1/2}$. The effective density is defined by $n_{eff} = \int n^2(\vec{r})\,dV \,/\, \int n(\vec{r})\,dV$, which is $n_0/8$ for an equilibrium distribution in a linear potential. The result is $\sigma = 6.0 \pm 3.0\ 10^{-12}\ cm^2$ for the elastic cross section. The estimated uncertainty mainly reflects three standard deviations of the fit with smaller contributions from the determination of density and temperature.

The measurement was performed at 200 μK, well below the temperature at which one expects d-wave contributions or a temperature dependence of the s-wave cross section [19, 20]. We can therefore deduce the scattering length $a = \pm(92 \pm 25)\ a_0$ using the relation $\sigma = 8\,\pi\,a^2$.

Recently, accurate calculations of the scattering length of cold sodium atoms have been performed[21, 22]. For sodium atoms in the F=1, $m_F = -1$ state the result was $56\ a_0 < a < 154\ a_0$ and, for an alternative choice of potentials $-36\ a_0 < a < 154\ a_0$ [21]. Thus negative values of the scattering length which would result in an unstable Bose condensate could not be ruled out. Our experimental result, together with the theoretical prediction, show that sodium in the F=1, $m_F = -1$ state has a large positive scattering length and is therefore an ideal choice for the pursuit of Bose Einstein condensation in alkali atoms.

In rf induced evaporation, atoms are spinflipped to an untrapped state when they are in resonance with an applied rf field. Because this resonance frequency is a function of magnetic field B, atoms are selectively removed at a specific value of B. In the case of transitions between magnetic sublevels m_F one has $\omega_{rf} = |g|\,\mu_B\,B/\hbar$, where g is the g-factor. Since the trapping potential is given by $m_F g \mu_B B(\vec{r})$, only atoms which have a total energy $E > \hbar\omega_{rf}\,|m_F|$ will evaporate, or in other words, application of rf radiation of frequency ω_{rf} creates a trap lip with a height of $\hbar\omega_{rf}\,|m_F|$. An advantage is that the "lip" exists over a large surface rather than a small saddle point region of the trap [6].

For a more detailed description of the evaporation process one has to use the dressed-atom formalism to obtain the eigenvalues of an atom in a combined magnetic and rf field. These solutions represent the adiabatic potential for the motion of the atoms. Slowly moving atoms follow the avoided crossing and stay on the lowest potential surface. The "spinflip" process is a two-photon adiabatic transition from a trapped to an untrapped state. If, as in our experiments, the strength of the rf magnetic field is not strong enough to ensure adiabaticity, one has to use Landau-Zener probabilities for spinflips at the avoided crossings. The evaporation of atoms saturates when the Landau-Zener probability is comparable to the ratio of oscillation time to equilibration time.

Forced evaporative cooling requires a continuous decrease of the potential depth to maintain it at an optimum value proportional to the decreasing temperature [12]. This was accomplished by ramping down the rf frequency. If the rf frequency changes too quickly, the atomic distribution is only truncated without increase in phase-space density; if it changes too slowly, more atoms than necessary are lost due to background gas collisions during the evaporation. The optimum result is obtained when the rf sweep keeps pace with the collisional thermalization [13, 23]. As discussed in Ref. [24] the phase space density increase in evaporative cooling is due to the combined effect of truncation and collisions, neither process alone would increase phase-space density.

Forced evaporation can also be obtained by adiabatically compressing the atoms at fixed rf frequency. We used a combination of both methods. After the initial loading a constant rf frequency of 30 MHz was applied and the magnetic field gradient increased by a factor of ten in 1 s. With the rf off, this increased the temperature by a factor of five whereas with evaporative cooling the temperature went up by only 20 %. Subsequently, the rf frequency was reduced linearly to 7 MHz within 200 ms. The temperature and density of the cloud was probed at various stages of the evaporation process after decompression to the initial field gradient. This ensured identical conditions for probing atoms and avoided very high optical densities and small clouds.

The results are shown in Fig. 2. We observed temperature reduction by a factor of 12 and a simultaneous increase in density by a factor of 4.6 resulting in an increased phase space density by a factor of 190. This means that the elastic collision rate, which is proportional to n v, was increasing during evaporation. At the intermediate stage of evaporation in Fig. 2, the elastic collision rate had doubled and then went down slightly, probably due to the loss of atoms by Majorana flops (see below). This means we are already in the regime of self-accelerating evaporation.

Indeed, one expects run-away evaporation when the number of collisions during a trapping time exceeds 25 [13]. With an estimated collision rate of 50/s in the compressed cloud we exceed this value by a factor of about 60. The cloud after evaporation had a temperature of 80 μK and a density of $2\ 10^{12}$ cm^{-3}, as inferred from 17 μK and $1.8\ 10^{11}$ cm^{-3} measured after adiabatic decompression. The uncertainties on temperarture and density are estimated to be 10% and 20 %, respectively. Our final phase space density is $2\ 10^{4}$ times smaller than required for Bose-Einstein condensation.

The current limitation of our evaporative cooling is an observed increased trap loss for small atom clouds. For the coldest temperatures achieved, the trapping time decreases from 30 s to a few seconds. This is most probably due to Majorana flops, non-adiabatic transitions to an untrapped state which happen in the center of the trap near the zero of the magnetic field. It may be shown that this loss rate is proportional to the ratio of the area of the "non-adiabatic" region around the center to the cross-sectional area of the cloud. From a Landau-Zener model we estimate the lifetime to be 500 d^2 (in seconds), where d is the cloud diameter in mm. The observed decrease in trapping time for cloud sizes of 100 μm is in qualitative agreement with this model.

In conclusion, we have evaporatively cooled alkali atoms and increased the phase space density by more than two orders of magnitude. We have achieved the initial conditions necessary for accelerated evaporation and identified non-adiabatic transitions in the center of the trap as the current limitation. Further progress should be possible after transferring

the atoms into a trap with a different field geometry which does not have zero magnetic field in the center.

This work was supported by the Office of Naval Research and Air Force Office of Scientific Research through grant N00014-90-J-1642, the Joint Services Electronics Program and the Sloan Foundation. M.-O.M. and K.B.D. would like to acknowledge support from Studienstiftung des Deutschen Volkes and the M.I.T. Physics Dept. Lester Wolfe fellowship, respectively. The authors are grateful to D.E. Pritchard for many useful discussions and to I.A. Entin for experimental assistance.

References

1 J. Lawall, F. Bardou, B. Saubamea, et al., Phys. Rev. Lett. **73**, 1915 (1994).

2 N. Davidson, H.-J. Lee, M. Kasevich, et al., Phys. Rev. Lett. **72**, 3158 (1994).

3 W. Ketterle, K. B. Davis, M. A. Joffe, et al., Phys. Rev. Lett. **70**, 2253 (1993).

4 T. Walker, D. Sesko, and C. Wieman, Phys. Rev. Lett. **64**, 408 (1990).

5 T. Walker and P. Feng, .

6 N. Masuhara, J. M. Doyle, J. C. Sandberg, et al., Phys. Rev. Lett. **61**, 935 (1988).

7 I. D. Setija, H. G. C. Werij, O. J. Luiten, et al., Phys. Rev. Lett. **70**, 2257 (1993).

8 K. B. Davis, M. O. Mewes, M. A. Joffe, et al., in *Fourteenth International Conference on Atomic Physics*, Boulder, Colorado, 1994).

9 W. Petrich, M. H. Anderson, J. R. Ensher, et al., in *Fourteenth International Conference on Atomic Physics*, Boulder, Colorado, 1994).

10 M. Kasevich, personal communication.

11 E. Tiesinga, A. J. Moerdijk, B. J. Verhaar, et al., Phys. Rev. A **46**, R1167 (1992).

12 H. F. Hess, Phys. Rev. B **34**, 3476 (1986).

13 K. B. Davis, M.-O. Mewes, and W. Ketterle, Appl. Phys. B **60**, 155-159 (1995).

14 D. E. Pritchard, K. Helmerson, and A. G. Martin, in *Atomic Physics 11*, edited by S. Haroche, J. C. Gay and G. Grynberg Proceedings of the 11th International Conference on Atomic Physics(World Scientific, Singapore, 1989), p. 179.

15 M. Drewsen, P. Laurent, A. Nadir, et al., Appl.Phys. B **59**, 283-298 (1994).

16 O. J. Luiten, H. G. C. Werij, I. D. Setija, et al., Phys. Rev. Lett. **70**, 544 (1993).

17 C. R. Monroe, E. A. Cornell, C. A. Sackett, et al., Phys. Rev. Lett. **70**, 414 (1993).

18 D. W. Snoke and J. P. Wolfe, Phys. Rev. B **39**, 4030 (1989).

19 A.-J. Moerdijk and B. J. Verhaar, personal communication.

20 This does not contradict the observation of d-wave scattering in recent photoasscocition experiments at 0.6 mK (L.P. Ratliff et al., J. Chem. Phys. 101, 2633 (1994)). Since the ratio of d- and s-wave partial cross sections scales as T^2 in inelastic scattering, the d-wave contribution to photodissociation at 0.2 mK should be less than 10%, and even smaller for elastic scattering which requires two passages through the centrifugal barrier.

21 A. J. Moerdijk and B. J. Verhaar, Phys. Rev. Lett. **73**, 518 (1994).

22 R. Côté and A. Dalgarno, Phys. Rev. A **50**, 4827 (1994).

23 J. M. Doyle, J. C. Sandberg, I. A. Yu, et al., Physica B 194-196, **13** (1994).

24 W. Ketterle and D. E. Pritchard, Phys. Rev. A **46**, 4051-4054 (1992).

Figure Captions

Figure 1

Thermal relaxation of an atom cloud after one-dimensional heating. The figure shows the time variation of the aspect ratio of the cloud for two different initial densities (solid circles: $5\ 10^{10}\ cm^{-3}$, open circles: $4\ 10^{9} cm^{-3}$). The lines represent simple exponential fits with time constants of 1.0 s and 13 s, respectively.

Figure 2

Optical density (a) and density (b) before and after evaporative cooling. (a): The initial cloud was cooled by adiabatic compression at constant rf frequency (middle trace) and further cooled by decreasing the rf frequency. The lines are fits to the observed profiles. The "bumpy" structure of the initial profile is a result of Zeeman shifts of the transitions used for probing the atoms. (b): Density before and after evaporation as obtained from the fits to the optical density profiles (temperatures are 200 μK and 17 μK, respectively).

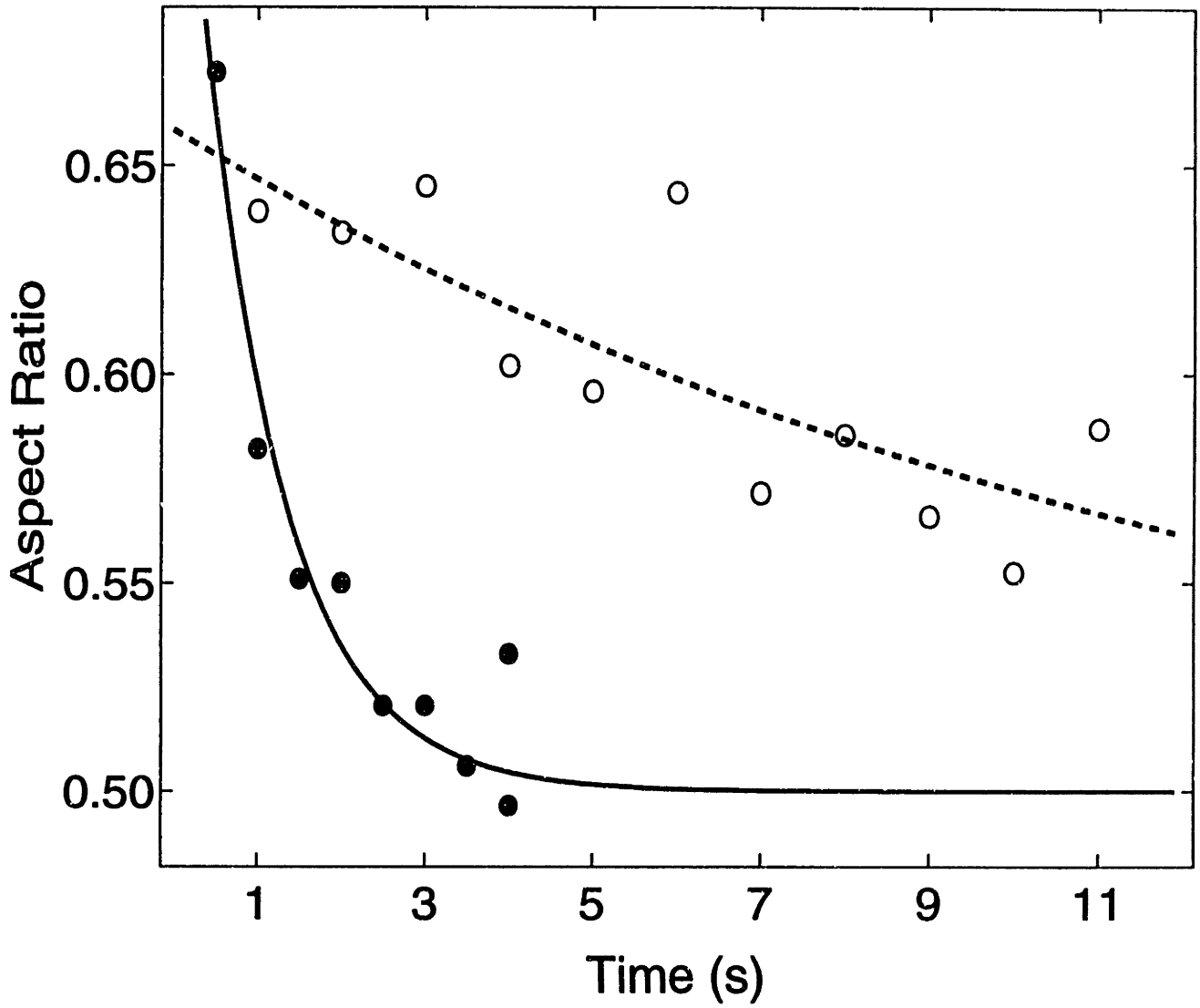

Figure 1

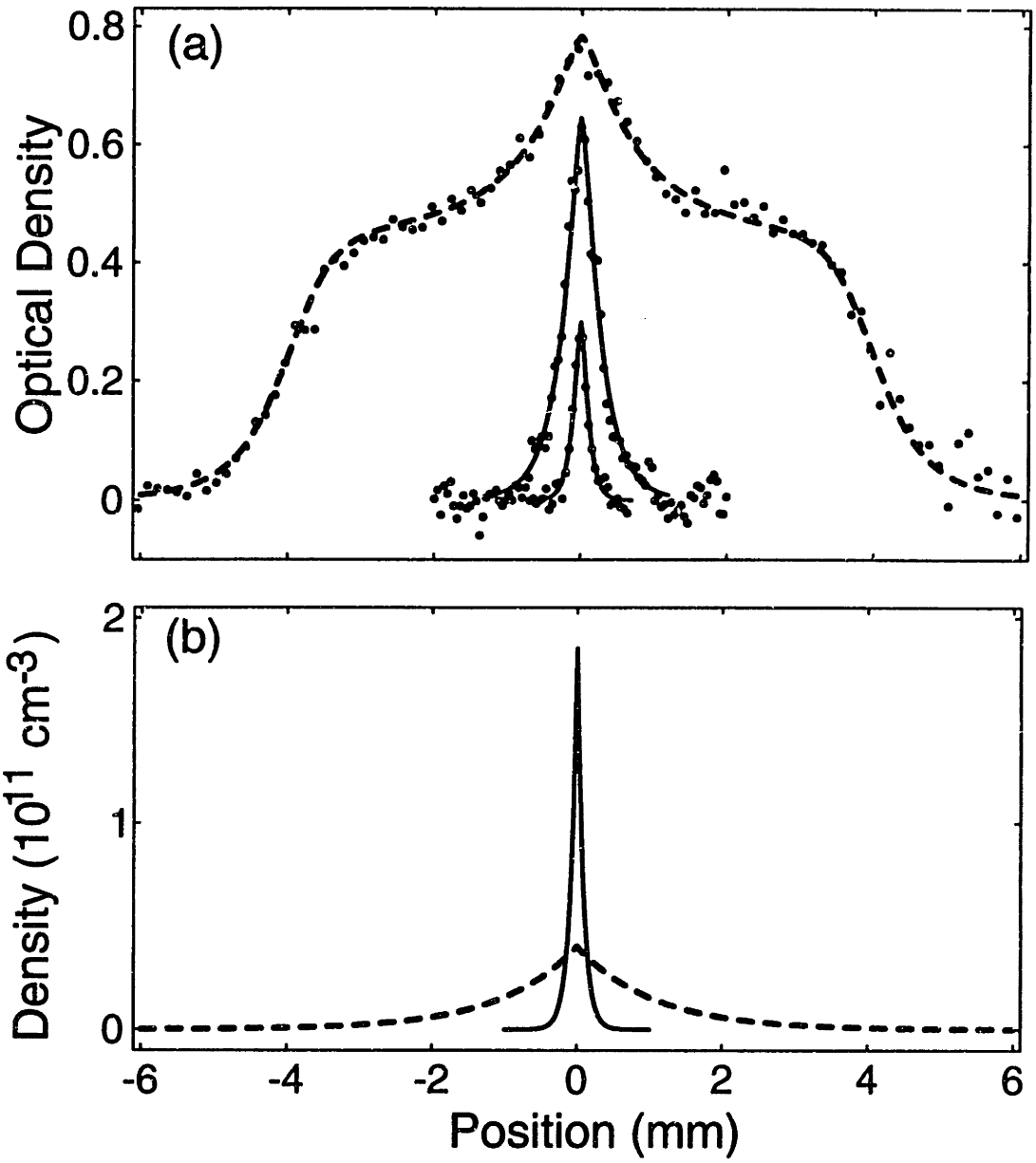
(a)
Optical Density
0.8
0.6
0.4
0.2
0
(b)
Density (10^{11} cm^{-3})
2
1
0
-6
-4
-2
0
2
4
6
Position (mm)

Figure 2

Chapter 4

An Optically Plugged Magnetic Quadrupole Trap

As indicated in the last chapter the major limitation to further evaporation in our magnetic quadrupole trap was a temperature dependent loss process (non adiabatic spin flips of atoms at the trap center). It is possible to estimate the size of the region in which atoms are lost by using classical arguments. When a dipole passes very close to the origin, the magnetic field experienced by the dipole may change direction faster than the dipole can follow. This process occurs when the rate of change of the magnetic field direction is comparable to the precession frequency.

Suppose that we have a particle on a trajectory near the origin with a closest approach distance equal to b (see fig 4.1)

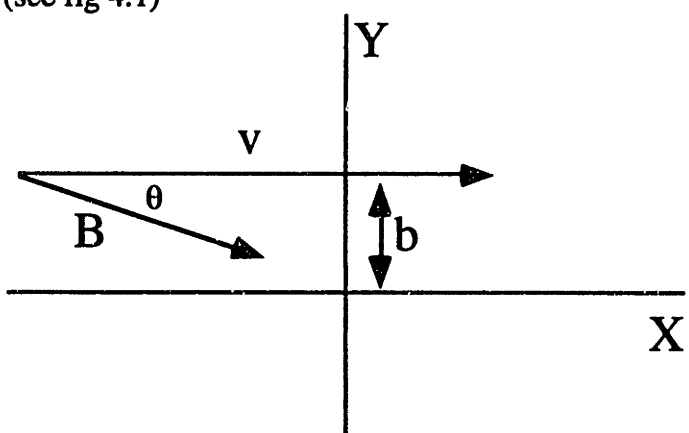

Figure 4.1 Particle velocity and magnetic field on a trajectory near the origin with distance of closest approach b. Theta is the angle between the local magnetic field direction and the velocity.

The magnetic field that this particle experiences as a function of position is given by $\vec{B} = B'\{-\vec{x}, -\vec{b}\}$.

Also we assume that the particle has a constant velocity given by

$\vec{v} = v_0 \hat{x}$.

The angle between the particle trajectory and the magnetic field is given by

$$\cos(\theta) = \frac{x}{\sqrt{x^2 + b^2}}$$

and thus

$$\frac{d\theta}{dt} = \frac{v_0}{b}\left(1 - \frac{x^2}{x^2 + b^2}\right).$$

The precession frequency in radians per second is

$$\omega_0 = \frac{\mu B' \sqrt{x^2 + b^2}}{\hbar}.$$

The critical point is at x=0, because the precession frequency has a minimum whereas dθ/dt has a maximum. Setting dθ/dt equal to ω_0 at x=0 we find the critical impact parameter b_c to be

$$b_c = \sqrt{\frac{\hbar v_0}{\mu B'}}.$$

This critical impact parameter is about 1 μm for B' = 1000 G/cm and v_0 = 1m/s (T = 1 mK). Using the exact quantum mechanical Landau Zener model [25] for avoided crossings we find a spin flip probability as a function of closest approach distance (b)

$$P = e^{-2\pi\left(\frac{b^2}{b_c^2}\right)}$$

The factor of two pi in the exponent indicates that there is effectively a hole in the center of the trap which is a fraction of a micrometer in diameter.

We will calculate the loss rate of atoms through this hole. Assume a cloud of atoms with characteristic dimension r_0 with a hole of characteristic dimension b_c. For a moment consider only those atoms that have velocities parallel to the x axis (see figure 4.2)

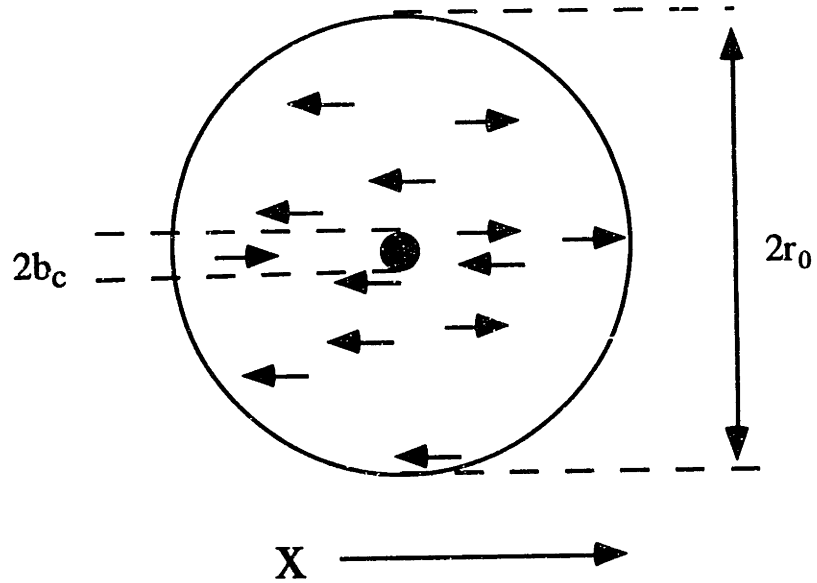

Figure 4.2. Atoms with velocity along the x direction in a cloud of radius r_0 with a hole of size b_c.

These atoms have a density distribution which is proportional to the total density distribution in the trap

$n(r) = n_0 e^{-r/r_0}$.

The number of these atoms that would be lost during one oscillation (N_{lost}) is equal to the number of these atoms found in a cylinder of radius b_c that extends from minus infinity to infinity. The fraction of these atoms that would be lost would be N_{lost} divided by the total number of atoms that have their velocity along the x direction. This fraction is independent of the direction of the velocity chosen.

Thus with this argument the loss rate per atom is

$$\Gamma = \frac{\int_{cylinder} (n(r))(2\nu_{osc})}{\int_{all} n(r)}.$$

In the above expression ν_{osc} is the oscillation frequency. There is a factor of 2 multiplying the oscillation frequency because the atom passes close to the origin twice per oscillation. Including the spatial variation of loss probability, p_{loss}, this expression becomes

$$\Gamma = \frac{\int_{all}(p_{loss})(n(r))(2v_{osc})}{\int_{all} n(r)}$$

We assume that the oscillation frequency is the same for all atoms in the cloud and that $b_c << r_0$. The numerator of this expression is calculated in cylindrical coordinates:

$$\int_{cylinder}(p_{loss})(n(r))(2v_{osc}) = \int_0^{\infty}\int_{-\infty}^{\infty} e^{-2\pi\rho^2/b_c^2} n_0 e^{-|z|/r_0} 2v_{osc} 2\pi(dz)(\rho d\rho) = 2v_{osc} r_0 b_c^2 n_0.$$

The denominator is also easily calculated

$$\int_{all} n(r) = \int_0^{\infty} n_0 e^{-r/r_0} 4\pi(r^2 dr) = 8\pi n_0 r_0^3.$$

Thus the loss rate is given by

$$\Gamma = \left(\frac{v_{osc}}{4\pi}\right)\left(\frac{b_c}{r_0}\right)^2.$$

Using

$$b_c^2 = \frac{\hbar v}{\mu B'}$$

and the virial theorem

$$\mu B' r_0 = mv^2$$

we can simplify Γ to obtain

$$\Gamma = \frac{\hbar}{4\pi m r_0^2}.$$

The lifetime ($1/\Gamma$) is then equal to

$$1/\Gamma = 1{,}000(r_0[mm])^2[s].$$

In the following sections we will examine the method by which we were able to make our trap lifetime independent of diameter and improve our phase space density by and additional two orders of magnitude.

4.1 AC Stark Shift Potential

Plugging the hole in the spherical quadrupole trap is accomplished by repelling atoms from the trap center using repulsive light forces. As will be shown below an atom's

potential energy increases when it is in the presence of light which is blue detuned from an atomic transition. By making the intensity of the blue detuned light a function of position it is possible to make a potential energy maximum. If we overlap this intensity maximum with the hole in the center of the magnetic quadrupole trap then atcms will not enter this region and the hole will be plugged.

A relatively simple model captures the physics behind the ac Stark shift potential. Consider the atom to be an electron attached to a spring. If we apply an external time dependent electric field then the equation of motion for the electron is

$$m\ddot{\vec{x}}_e + m\omega_0^2\vec{x}_e = -e\vec{E}(\vec{x},t).$$

Where ω_0 is the resonance frequency of the mass spring system and x_e is the position of the electron. We assume that we are in a regime that damping of the mass spring system is negligible, but we will justify this point later. The solution for an electric field of the form

$$\vec{E}(\vec{x},t) = \hat{\varepsilon}E(\vec{x})\sin(\omega t)$$

is

$$\vec{x}_e = \hat{\varepsilon}x_0\sin(\omega t)$$

where x_0 is given by

$$x_0 = \frac{eE(\vec{x})}{m(\omega^2 - \omega_0^2)}.$$

Therefore the atom has a time varying dipole moment induced by the electric field

$$\vec{p} = -e\vec{x}_e.$$

This dipole moment gives rise to a time averaged potential equal to

$$\langle U\rangle = \left\langle -\vec{p}\cdot\vec{E}\right\rangle = \frac{e^2E^2(\vec{x})}{2m(\omega^2 - \omega_0^2)}.$$

The exact quantum mechanical expression is related to the classical expression given above through

$$\langle U_{QM}\rangle = f_{fi}\langle U_{Class}\rangle$$

f_{fi} is the oscillator strength of the transition. In the case of the sodium D line the oscillator strength is very close to unity, so the classical expression is an excellent approximation.

In order to keep atoms away from the center of the trap with this light shift potential, we would like to maximize U. For finite laser power, this is achieved by focusing the laser light very tightly. The hole we want to plug is only a micrometer in diameter, therefore tightly focusing the laser light does not have any adverse effects.

For argon ion laser light at 514 nm the light shift has the following dependence on intensity

$$\frac{U}{h} = 3 \cdot 10^3 MHz \times I\left[\frac{W}{(\mu m)^2}\right].$$

Typical parameters are one Watt light focused down to a 10 micrometer (FWHM) beam waist. The light shift potential is 30 MHz which is sufficient to plug the hole.

The combined magnetic, light shift and rf potential is displayed in figure 4.3

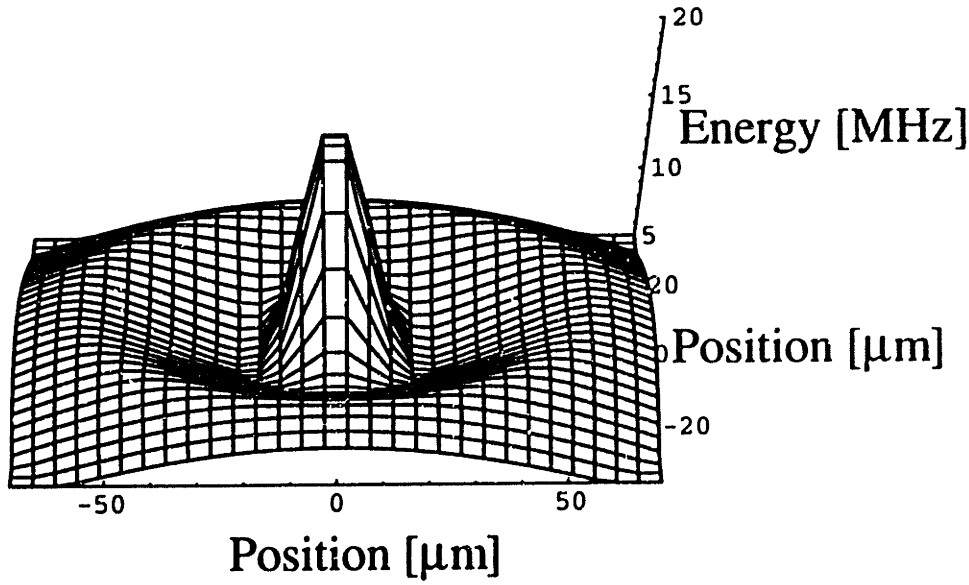

Figure 4.3 The total potential including the optical plug, the magnetic field and the rf. The potential is not cylidrically symmetric due to the fact that the magnetic field gradient is twice as strong along the axis going into the page.

4.2 Photon Scattering

In the previous model we neglected the damping of the mass spring system. The quantum mechanical realization of classical damping is spontaneous emission of photons. It is important that the light for the optical plug is far enough detuned from any atomic transition that the photon scattering rate is small in comparison to the evaporation rate. Evaporative cooling takes typically a few seconds, thus the photon scattering rate should be less than 0.1 Hz. An atom in the presence of light far detuned from resonance scatters photons at a rate

$$\gamma_s = \Gamma \frac{\omega_R^2}{4\delta^2},$$

where Γ is the natural decay rate of the transition, ω_R is the Rabi frequency, and δ is the detuning. In the optically plugged magnetic trap the Rabi frequency (which is proportional to intensity) is a function of position. For 1 Watt of light at 514 nm and focused down to a 10 micrometer beam waist the scattering rate is

$$\gamma_s = 4.01 e^{(-x^2/100)} [Hz] .$$

x is in units of micrometer and x = 0 is the center of the laser beam.

Atoms in the trap move and are therefore exposed to a time dependent laser intensity. For atoms moving in one dimension along a radial orbit (so that once per period they are repelled from the center of the trap by the laser light). The average scattering rate is the number of photons scattered per orbit divided by the orbital period.

$$\langle \gamma_s \rangle = \frac{\int_{orbit} \gamma_s dt}{\int_{orbit} dt}.$$

This integral is transformed to a position space integral using the substitution

$$dt = \frac{dx}{\sqrt{\frac{2}{m}(E - U(x))}}$$

where E is the total energy of the particle and U(x) is the position dependent potential.

$$\langle \gamma_s \rangle = \frac{\int_{x_{inner}}^{x_{outer}} \frac{4.01 e^{-x^2/100} dx}{\sqrt{\frac{2}{m}(E - U(x))}}}{\int_{x_{inner}}^{x_{outer}} \frac{dx}{\sqrt{\frac{2}{m}(E - U(x))}}}$$

where x_{inner} is the inner turning point of the orbit and x_{outer} is the outer turning point of the orbit. The results of this calculation are shown in figure 4.4.

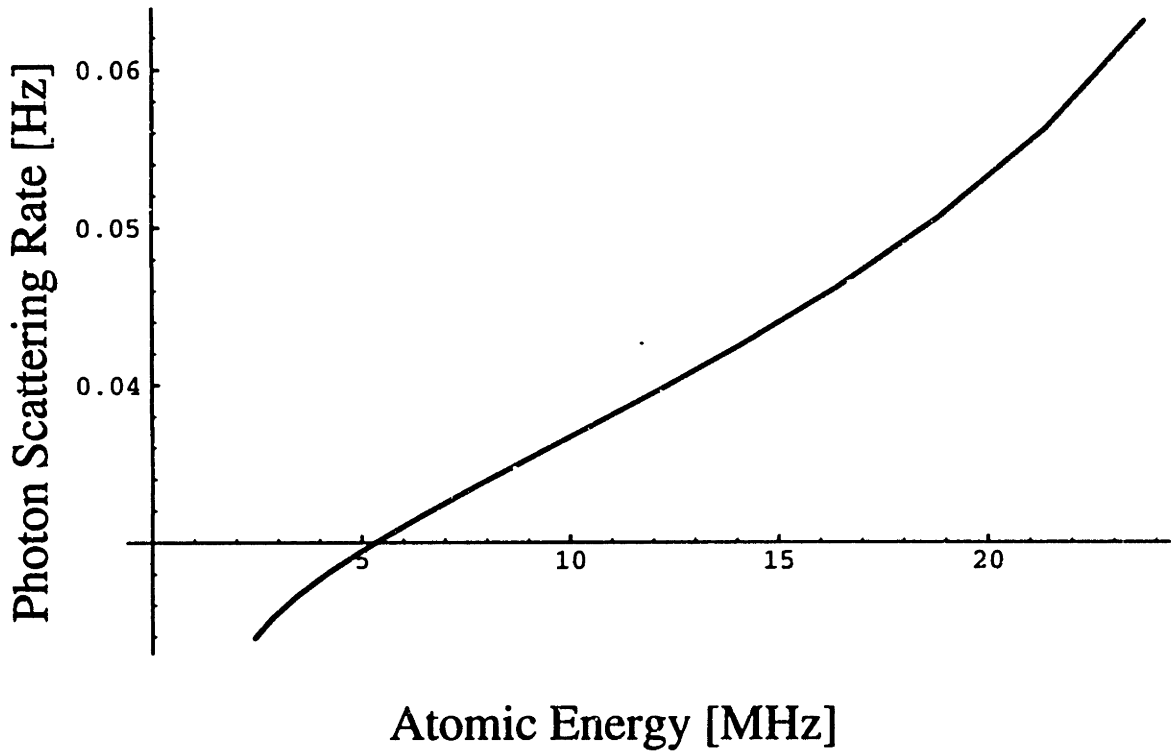

Figure 4.4 The average photon scattering rate vs. total energy of the atom. The more energy an atom has the more laser light is required to change the atom's direction The average photon scattering rate is therefore an increasing function of atomic energy.

We can see from the plot that even for energies as high as 20 MHz the photon scattering rate is below 0.1 Hz. This calculation provides an upper bound on the scattering rate in a three dimensional potential because not all atoms are on a radial orbit. In addition this calculation was carried out along the symmetry axis of the trapping coils where the field gradient is twice as large as along the other two axes. This is significant because atoms moving along the symmetry axis are confined to half the radial distance from the origin and thus sample the region of intense laser light more frequently.

We are in a regime were the laser detuning is much greater than the fine structure splitting of the (3P) excited state. This has the following consequence, an atom which is excited and spontaneously emits a photon it is much more likely to return to its initial state (the trapped state) than it is to be optically pumped to an untrapped state. Therefore to leading order photon scattering is a heating process not a loss mechanism. The heating rate is proportional to the photon scattering rate and is found to be 20 nK/s at a temperature of 10 μK.

4.3 Experimental Results

Employing the repulsive AC Stark shift potential to keep atoms away from the trap center we were able to improve on the initial demonstration of evaporation detailed in the last chapter. Indeed the optically plugged magnetic trap proved to be an ideal environment to continue evaporation. In this new trap we were able to achieve atomic densities of 3 10^{13} cm^{-3} and temperatures of 10 μK. A 10 μK fully compressed cloud has a diameter of 10 μm. The smallest features which we could clearly resolve with our diffraction limited optical system was 8 μm. We therefore concluded that optical resolution was the major limitation to further cooling. A more detailed description of the results of this experiment are presented in the appendix to chapter 4.

Appendix to Chapter 4

In the following section a paper is presented which will be submitted to *Physical Review Letters.*

Improved Evaporative Cooling in an Optically Plugged Magnetic Quadrupole Trap

Kendall B. Davis, Marc-Oliver Mewes, Michael R. Andrews,

and Wolfgang Ketterle

Department of Physics and Research Laboratory of Electronics

Massachusetts Institute of Technology, Cambridge, MA 02139

Abstract

We have demonstrated a novel type of magnetic trap, which provides the tight confinement of a linear potential, but avoids trap loss due to non-adiabatic spin flips near zero magnetic field. The trap loss is suppressed by a tightly focused blue detuned laser beam which creates a repulsive AC Stark shift potential around the zero of the magnetic field. Rf induced evaporation in this trap increased the phase space density by four orders of magnitude, only a factor of 30 less than the phase transition to Bose-Einstein condensation.

PACS: 32.80.Ps, 42.50.Vk

With recent advances in laser cooling, atomic samples can be cooled below the recoil limit[1,2]. Collisions and absorption effects limit the atomic density to about 10^{12} cm^{-3}; the highest phase-space density achieved is still three orders of magnitude smaller than required for the observation of quantum-statistical effects. Because of these limitations, several research groups have focused on evaporative cooling. This method originally developed for atomic hydrogen[3,4], requires collisional thermalization times which are much less the lifetime of the sample. This was achieved for alkali atoms only very recently[5-7].

Evaporative cooling requires an atom trap which is tightly confining and does not have any inherent loss mechanisms. So far magnetic traps and optical dipole traps have been used. Dipole traps are tightly confining, but have only a very small trapping volume (10^{-8} cm^3). The tightest confinement is a magnetic trap is achieved with a linear (spherical quadrupole) potential (see below), however this potential suffers from trap loss due to non-adiabatic spinflips. A recently demonstration ac magnetic trap suppresses this trap loss, but has less confinement. In this paper we present a novel atom trap which combines magnetic forces and optical dipole forces and offers a superior combination of large trapping volume and tight confinement. In such a trap we observed greatly improved evaporative cooling, increasing the phase space density by more than four orders of magnitude.

We would like to discuss in some detail why a linear potential is superior to a quadratic potential for evaporative cooling. First, it provides the same confinement with lower fields, B_0 at the coils. B_0 is approximately given by $\mu B_0 (d/R)^n = kT$. where R is the radius of the trap coils, r the radius of the atom cloud at a temperature T, μ is the magnetic moment of the atom, and n the exponent of the power-law potential. R/r is typically larger than ten to ensure optical access to the trapped cloud. Linear confinement therefore requires more than ten times smaller B_0, or if larger B_0 are available, as in our experiments, they can be used to adiabatically compress the cloud and speed up evaporative cooling by more than an order of magnitude.

The second advantage of the linear potential is the rapid increase in density during evaporation. The volume of a trapped sample is proportional to $T^{3/n}$. Both effects make it much easier to meet the condition for self-accelerating evaporation[8]. The necessary product of initial density times trapping time is two orders of magnitude lower for a linear potential.

In all magnetic traps the magnetic field direction changes as a function of position and thus for an atom to remain confined in the trap the atom's magnetic dipole moment must adiabatically follow the local magnetic field direction. Roughly the condition for the atom to adiabatically follow is that the atom's precession frequency ($\mu B/h$) be greater than the rate of change of the magnetic field direction. In the magnetic quadrupole trap the precession frequency is small near the origin. The change in the magnetic field direction, for an atom with a given velocity, is large near the origin.

Thus in the vicinity of the origin there exists a small critical volume, a "hole", an atom entering this volume will be lost. The characteristic radius (b_0) of this volume depends on the field gradient and the velocity of the atom $b_0 \sim (vh/\mu B')^{1/2}$ [9, 10]. A more exact treatment of this loss mechanism is described by the Landau-Zener model for avoided level crossings[11]. This model predicts that the atom's probability of a non-adiabatic transition is given by

$$P(y) = e^{-2\pi \frac{y^2}{b_0^2}} \qquad (1)$$

where y is the distance of closest approach of the atom to the origin. For sodium atoms at 100 μK in a magnetic trap with a gradient of 1000 G/cm then the typical dimension b_0 of the hole is well below one micrometer. As atoms in the trap cool, they occupy a volume which decreases with the third power of the temperature, whereas b_0 decreases only with the fourth root of the temperature. Therefore these non-adiabatic transitions become a dominant loss mechanism at low temperatures. From a Landau-Zener model we estimate the lifetime to be 500 d^2 (in seconds), where d is the cloud diameter in mm.

The trap loss can be suppressed by adding a repulsive potential around the zero of the magnetic field. This is accomplished by tightly focusing an intense blue detuned laser. If the detuning δ ($\delta = \omega_L - \omega_0$) between the laser ($\omega_L$) and the atomic frequency (ω_0) is much larger than the natural linewidth (Γ), then the dipole force potential is given by[12]

$$U(\mathbf{r}) = \frac{\hbar\Gamma^2}{8\delta}\left(\frac{I(\mathbf{r})}{I_0}\right). \qquad (2)$$

$I(\mathbf{r})$ is the local intensity of the laser, I_0 is the saturation intensity.

The total potential experienced by the atoms is a combination of the dipole potential, the quadrupole trapping potential and the rf dressed atom potential. The latter can be understood qualitatively with a simple argument. At the point where atoms are in resonance with the rf ($r=\hbar\omega_{rf}/\mu B'$) the trapped state undergoes an avoided crossing with the untrapped states, as a result the trapping potential bends over. The total potential orthogonal to the propagation direction of the blue detuned laser is depicted in figure 1.

One concern when using light forces to manipulate atoms is the heating generated by photon scattering. For $\delta >> \Gamma$ the photon scattering rate is equal to $(\Gamma^3 I(\mathbf{r}))/(8\delta^2 I_0) = (U(\mathbf{r})\Gamma)/(\hbar\delta)$. Thus a convenient way to suppress the scattering is to use laser light far detuned from resonance[13, 14]. An additional suppression in the photon scattering rate can be gained by using blue detuned light because the atoms are repelled from the region where the laser intensity is high[15].

We have numerically calculated the photon scattering rate for an atom moving radially in the potential depicted in figure 1. The photon scattering rate is less than 0.1 Hz at 1 mK and drops roughly linearly with the temperature. At about 15 μK atoms settle down into the minima of the potential (see figure 1) and the photon scattering rate becomes constant at about 0.02 Hz. It should be noted that only a small fraction of the photons scattered result in trap loss. The laser detuning is much larger than the excited state fine structure splitting, thus it is very unlikely that a scattering event will change the polarization of the atom[16].

The heating rate due to photon scattering is less than 20 nK/s ($T < 10\ \mu K$) and thus is completely negligible for the current experiment.

The basic experimental setup was similar to that described in reference[7]. A high density of magnetically trapped atoms is obtained in a multistep procedure. Atoms were initially slowed in a Zeeman slower and loaded into a Dark SPOT [17]. Typically, 10^9 to 10^{10} atoms were confined at densities of $5\ 10^{11}\ cm^{-3}$. Sub-Doppler temperatures of $100 \Leftrightarrow \mu K$ were achieved by turning off the weak quadrupole magnetic field and applying a dark version of polarization gradient cooling. In situ loading of the magnetic trap was accomplished by extinguishing the laser light quickly (< 1 ms) and applying magnetic quadrupole field of 100 G/cm. The density in the magnetic trap is a factor of ten lower than in the light trap because only about one third of the atoms are in the trapped F=1, $m_F = -1$ state, and because of some expansion of the cloud. Subsequently, the magnetic field gradient was adiabatically increased to 1000 G/cm increasing the density by a factor of ten and the temperature by a factor of five. The sample of atoms prepared in this way had typically $8\ 10^8$ atoms at a peak density of $5\ 10^{11}\ cm^{-3}$ and a temperature of 1 mK.

This sample was then cooled by rf induced evaporation[5, 7, 18]. Atoms with the highest total energy are spinflipped to non-trapped states. Density, temperature and total number of atoms were determined using in situ absorption imaging. Absorption images were compared to numerical simulations of the propagation of polarized light through a spin-polarized sample in an inhomogeneous magnetic field[19]. Identical results were obtained from two successive images insuring that the absorption imaging was non-perturbative.

The only significant modification to our previous experimental setup was the addition of a 3 Watt argon ion laser beam (514 nm) focused to a beam waist (FWHM) of 8 μm. This beam waist was spatially overlapped with the center of our magnetic trap and provided about 90 MHz of light shift potential at the origin.

The optical plug had to be aligned with μm precision. The position of the plug could be determined by the depletion of the atomic density (see figure 2). However, for cloud sizes

of > 100 μm, the depletion could only be observed collinear with the Ar ion laser beam due to the line of sight integration of absorption imaging. Smaller cloud sizes could only be achieved after the plug was well aligned. To detect the weak probe beam, which was collinear with the Ar ion laser beam, required suppressing the green light by 15 orders of magnitude. This was accomplished with a dichroic mirror, a crossed polarizer and an absorptive edge filter in series. These optics attenuated the yellow probe light by a factor of two.

We have measured the lifetime both with and without the optical plug for various diameters of the cloud.. The temperature and thus the diameter of the cloud was varied by using rf induced evaporation[5, 7]. To insure that we have identical samples for comparison a cloud of atoms with a given diameter was prepared using the optical plug, the lifetime in the quadrupole potential was determined by rapidly switching off the blue detuned light. The results shown in figure 3 demonstrate that Majorana spin flips are completely suppressed with the optical plug. The lifetime of cloud with the optical plug is predominantly limited by background gas collisions. A misalignment of the optical plug by a few μm resulted in increased trap loss. This is the final evidence that the Majorana spin flips are localized in a very small region around the center of the trap.

In our previous demonstration[7] we were able to cool from an initial temperature of 1 mK to a final temperature of 85 μK by sweeping the rf from 30 to 4 MHz. Using the optically plugged magnetic quadrupole trap we could continue evaporation down to an rf frequency of 1 MHz. This evaporation resulted in clouds that had an optical density of 150 (see figure 4) and a diameter along the symmetry axis of the coil of 20 μm (see figure 2). This corresponds to a density of $3.6 \cdot 10^{13}$ cm^{-3} and temperatures of 10 μK. This combination is a factor of 500 improvement over our previous results[7]. The elastic collision rate at this point is a factor of 7 higher than at our starting point $5\ 10^{11}$ cm^{-3} and 1 mK and is estimated to be about 200 Hz. Thus we are strongly in the regime of self

accelerating evaporation. The highest phase space densities achieved are a factor of 30 lower than required for Bose-Einstein condensation.

When atoms cool below 15 μK at a gradient of 1000 G/cm in the optically plugged magnetic quadrupole trap they settle down into the two spatially separated minima of the total potential, see figure 2 and figure 3. We were unable to continue the cooling below 10 μK because the cloud became smaller that the resolution of the imaging system (see figure 3).

A second limitation to the to the ultimate temperature comes from the vibrational motion of the plug with respect to the zero of the magnetic field. A displacement Δx of the laser's beam waist changes the magnetic field at the bottom of the potential by $(1/2)B'\Delta x$, where B' is the gradient along the symmetry axis of the coils. For constant rf frequency, the trap depth changes by $(g/2)\mu_B B'\Delta x$, where g is the g factor of the trapped state and μ_B is the Bohr magneton. An estimated Δx of about 2μm, results in fluctuations of the potential depth of 4μK, preventing cooling much below 10 μK.

Both limitations are mitigated by adiabatic decompression. Preliminary attempts to expand the cloud by lowering the field gradient failed. This is largely due to the fact that the magnetic trapping coils moved about 50 μm along their symmetry axis when the current was varied between 0 and 300 A. Attempts to compensate for this with additional coils were only partially successful, probably due to some irregular motion on the μm scale. A more fundamental limitation is that the characteristic dimension of the non-adiabatic region increases with decreasing field gradient.

These limitations can be avoided by using a light sheet to sweep the atoms away from the hole by a distance of about 50 μm. Such a large displacement would make the atomic sample relatively insensitive to the exact position and size of the hole. Such experiments are currently in preparation.

In conclusion, we have evaporatively cooled alkali atoms in a novel optically plugged magnetic trap. In this trap we have witnessed strongly self accelerating evaporation and

phase space densities a factor of thirty lower than required to observe B.E.C. The current limitation is the small size of the cloud, and further improvements are expected using adiabatic decompression in a modified trapping geometry.

This work was supported by the Office of Naval Research through grant N00014-90-J-1642, the Joint Services Electronics Program and the Sloan Foundation. M.-O.M. and K.B.D. would like to acknowledge support from Studienstiftung des Deutschen Volkes and M.I.T. Physics Dept. Lester Wolfe fellowship, respectively.

References

1 M. Kasevich and S. Chu, Phys. Rev. Lett. **69**, 1741 (1992).

2 J. Lawall, F. Bardou, B. Saubamea, *et al.*, Phys. Rev. Lett. **73**, 1915 (1994).

3 H. F. Hess, Phys. Rev. B **34**, 3476 (1986).

4 N. Masuhara, J. M. Doyle, J. C. Sandberg, *et al.*, Phys. Rev. Lett. **61**, 935 (1988).

5 W. Petrich, M. H. Anderson, J. R. Ensher, *et al.*, in Phys. Rev. Lett..

6 M. Kasevich, personal communication.

7 K. B. Davis, M.-O. Mewes, M. A. Joffe, *et al.*, in Phys. Rev. Lett..

8 K. B. Davis, M.-O. Mewes, and W. Ketterle, App. Phys. B **60**, 155-159 (1995).

9 A. L. Migdall, J. V. Prodan, W. D. Phillips, *et al.*, Phys. Rev. Lett. **54**, 2596 (1985).

10 W. Phillips, J. Prodan, and H. Metcalf, J. Opt. Soc. Am. B **2**, 1751 (1985).

11 J. Rubbmark, Kash,M. et al., Phys. Rev. A **23** (1981).

12 A. Ashkin, Phys. Rev. Lett. **40**, 729 (1978).

13 J. D. Miller, R. A. Cline, and D. J. Heinzen, Phys. Rev. A **47**, R4567 (1993).

14 W. D. Phillips, in *International School of Physics*, edited by E. Arimondo, W. Phillips and F. Strumia (Elsevier Science Publishing Co. Inc., Varrenna, 1991), p. 289.

15 N. Davidson, H. J. Lee, C. S. Adams, *et al.*, Phys. Rev. Lett. **74**, 1311 (1995).

16 R. Cline, J. Miller, M. Matthews, *et al.*, Opt. Lett. **19**, 207 (1994).

17 W. Ketterle, K. B. Davis, M. A. Joffe, *et al.*, Phys. Rev. Lett. **70**, 2253 (1993).

18 D. E. Pritchard, K. Helmerson, and A. G. Martin, in *Atomic Physics 11*, edited by S. Haroche, J. C. Gay and G. Grynberg (World Scientific, Singapore, 1989), p. 179.

19 O. J. Luiten, H. G. C. Werij, I. D. Setija, *et al.*, Phys. Rev. Lett. **70**, 544 (1993).

Figure Captions

Figure 1

Adiabatic potential due to the magnetic quadrupole field, the optical plug, and the rf. Distances along the X and Y axis are measured in micrometer. This cut of the three dimensional potential is orthogonal to the propagation direction of the blue detuned laser.

Figure 2

Absorption images of atoms confined in an optically plugged magnetic quadrupole trap. (a) Large atomic samples (T 40 μK) have a two to one aspect ratio because the gradient along the vertical axis is twice as large as it is along the horizontal axis. (b) Colder atoms (T 15 μK) are confined to the two spatially separated minima of the potential. (c) For T< 10 μK the cloud is smaller than the resolution of our optical system.

Figure 3

Final data to be taken.

Figure 4

Absorption spectrum of sodium atoms trapped in an optically plugged magnetic trap. The zero of the frequency scale corresponds to the (3S) F=1 to ($3P_{3/2}$) F=2 transition. The diameter of the cloud is 20 μm along the strong (vertical) axis of the magnetic field corresponding to a temperature of 15 μK. The best fit yields an optical density of 150 which corresponds to an atomic density of $3.6\ 10^{13}$ and ~ $2\ 10^{6}$ trapped atoms.

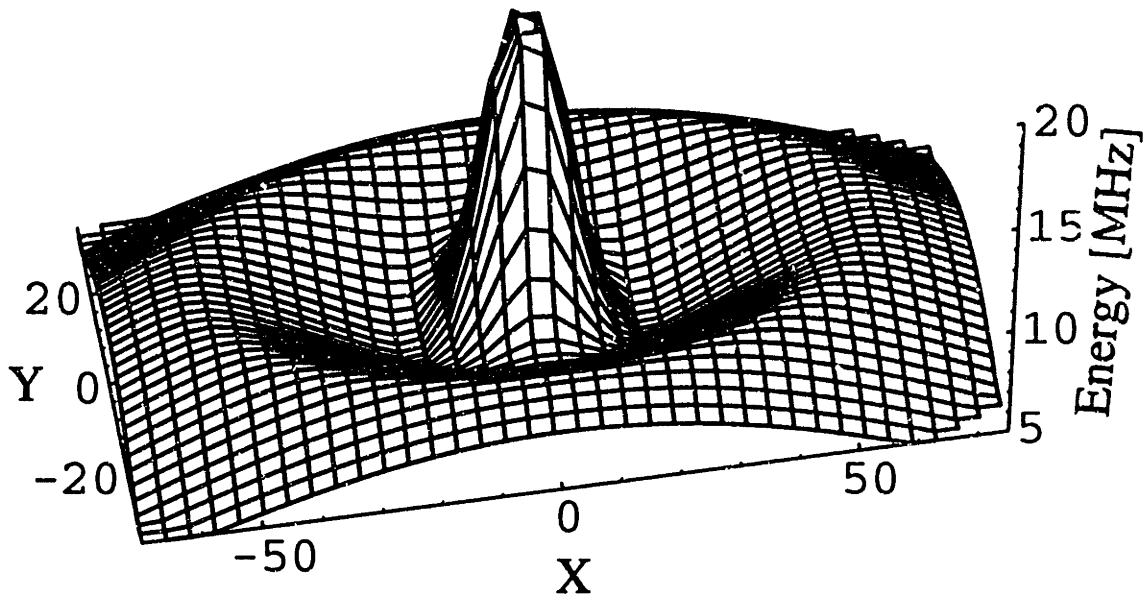

Figure 1

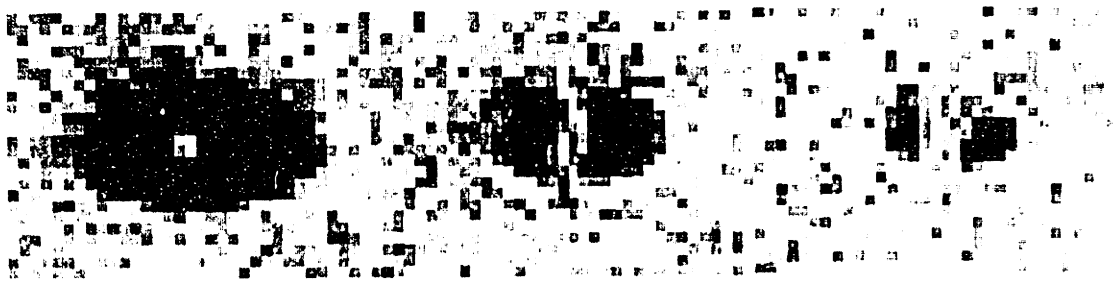

(a) (b) (c)

Figure 2

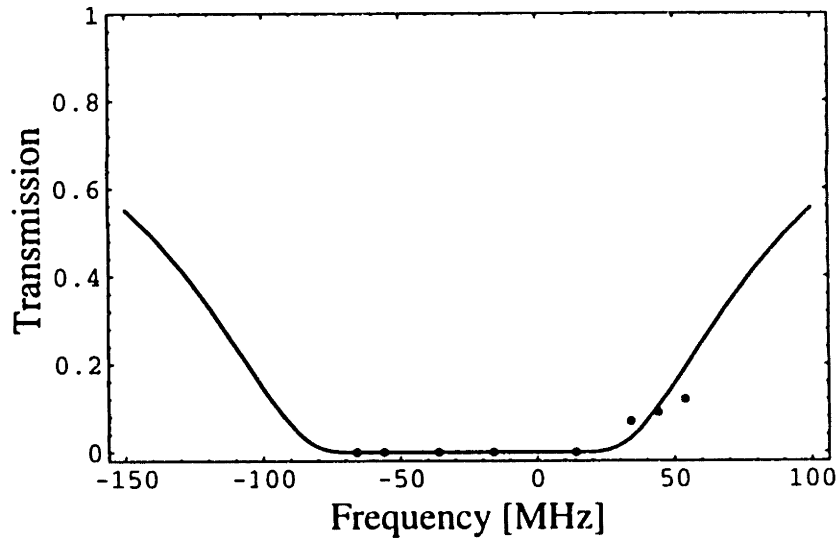

Figure 4

Chapter 5
Light Sheet Traps

As was discussed briefly at the end of the last chapter a cold (10 μK) sample of atoms in the optically plugged magnetic trap is too small to optically resolve. In addition there is also another detection problem associated with such small dense clouds.

5.1 The Spatial Distribution of a Bose Condensate

In order to detect a Bose condensate we must insure that it has a spatial distribution which is different than that of the remaining thermal gas. In the following section the density dependence of the condensate's energy and the effect that the energy has on the spatial distribution will be examined. In addition a density, temperature combination will be determined which is optimal for detection.

A sodium atom colliding with another sodium atom acts to a large extent like a billiard ball. It has a short range repulsive potential characterized by its scattering length. At high densities this short range repulsive potential will contribute to the average total potential that an atom experiences in a significant way. In mean field theory[1, 27].the effective potential that an atom experiences is given by

$$V_{mf} = \left(\frac{4\pi\hbar^2 a}{m}\right)n.$$

where a is the scattering length and n is the density.

For sodium the quantity in parentheses is equal to 1.2 10^{-15} μk cm^3. The size of a condensate can be estimated in a self consistent way by requiring that the mean field energy of the condensate is equal to the average potential energy of the condensate

$$2V_{mf} = 1/2kr^2.$$

$$2\left(\frac{4\pi\hbar^2 a}{m}\right)\frac{3N}{4\pi r^3} = 1/2kr^2$$

k is the curvature of the harmonic potential. If we assume N (the total number of atoms in the condensate) to be 10^4 and k to be 0.02 kHz/μm^2 then r is equal to 10 μm. This would give rise to a condensate with a density of 10^{13} cm^{-3}. This is a desirable density range for the condensate because at densities of 5 10^{14} cm^{-3} we expect dipolar relaxation to become a dominant loss mechanism[27].

We expect to diagnose a Bose condensate by imaging the spatial distribution of the condensate and the remaining thermal atoms. We anticipate that as we cross the transition line a narrow peak (the condensate) will emerge inside the spatial profile of the thermal distribution. If the size of the thermal distribution is comparable to the size of the condensate then it is difficult to detect the condensate. Thus it is advantageous to work at relatively low densities. If we were to cross the transition line at a density of 10^{12} cm^{-3} and temperature of 100 nK (again taking U = 1/2kr^2; k = 0.02 kHz/μm^2) then the condensate would have a linear dimension three times smaller than the thermal distribution which should be easy to detect (see figure 5.1).

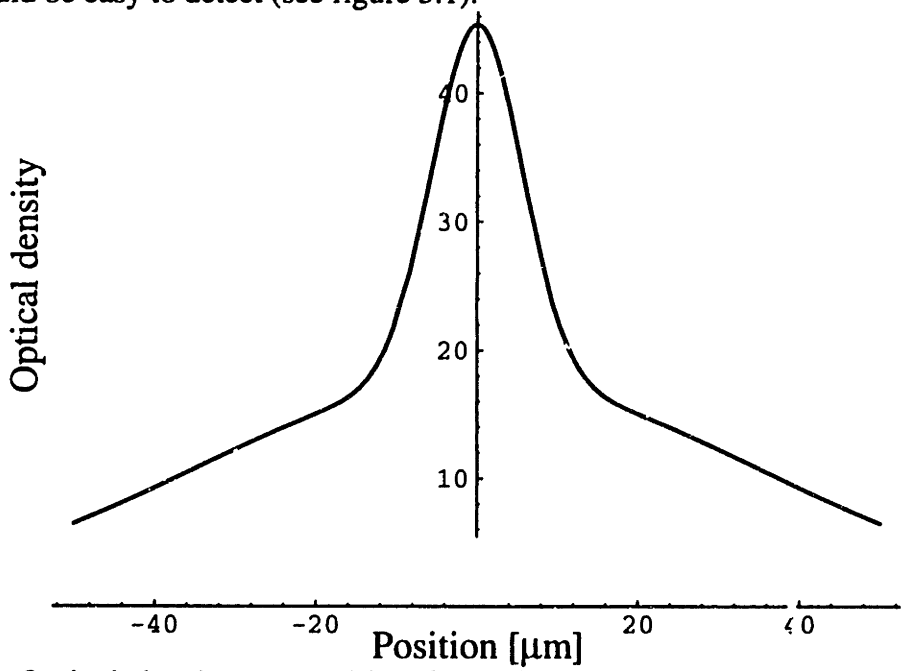

Figure 5.1 Optical density vs. position for a thermal cloud and a Bose condensate, assuming 50% of the atoms are in the condensate.

Thus there are two good reasons for us to enlarge the size of our cloud. This can be accomplished by simply decompressing the cloud. Unfortunately the trapping coils moved as we changed the field gradient (at 300 Amps they repelled each other with a force of 50 N). As a result the zero of the magnetic field moved by 50 μm along the symmetry axis of the coils when the gradient was varied from 0 to 1000 G/cm. Our initial attempts to decompress the cloud were to a large extent a failure because we were unable to fully compensate for the motion of the magnetic field zero (we suspect some irregular motion of the field zero on the micrometer scale).

A solution is the light sheet trap. This trap is similar to the optically plugged magnetic trap except that the laser beam has an asymmetric focus with an aspect ratio of 5 to 1 (such a focus is commonly referred to as a light sheet). If this new plug has its long axis aligned with the symmetry axis of the coils then decompression is possible even if the zero of the magnetic field is moving.

5.2 Advantages of the Light Sheet Trap

There are a few additional reasons to use the light sheet trap instead of the optically plugged magnetic trap. If after cooling the atoms to the point that they form two independent clouds we displace the zero of the magnetic field perpendicular to the plane of the light sheet then the atoms that are caught in the pocket formed by the light sheet and the magnetic field (see figure 5.2) are all spin polarized in almost the same direction (see figure 5.3). They are also sampling a rather large magnetic field and thus the probability of Majorana spin flips is reduced by an enormous factor.

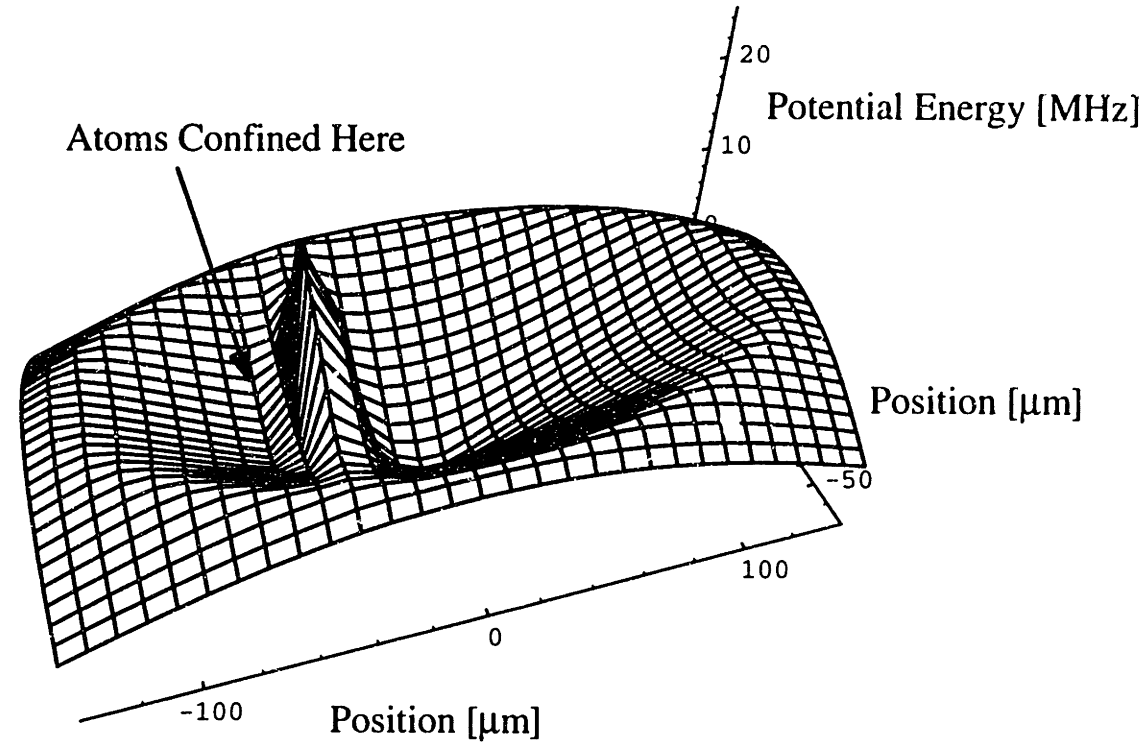

Figure 5.2 The light sheet displaced from the origin in conjunction with the magnetic field forms a local potential minimum which confines atoms.

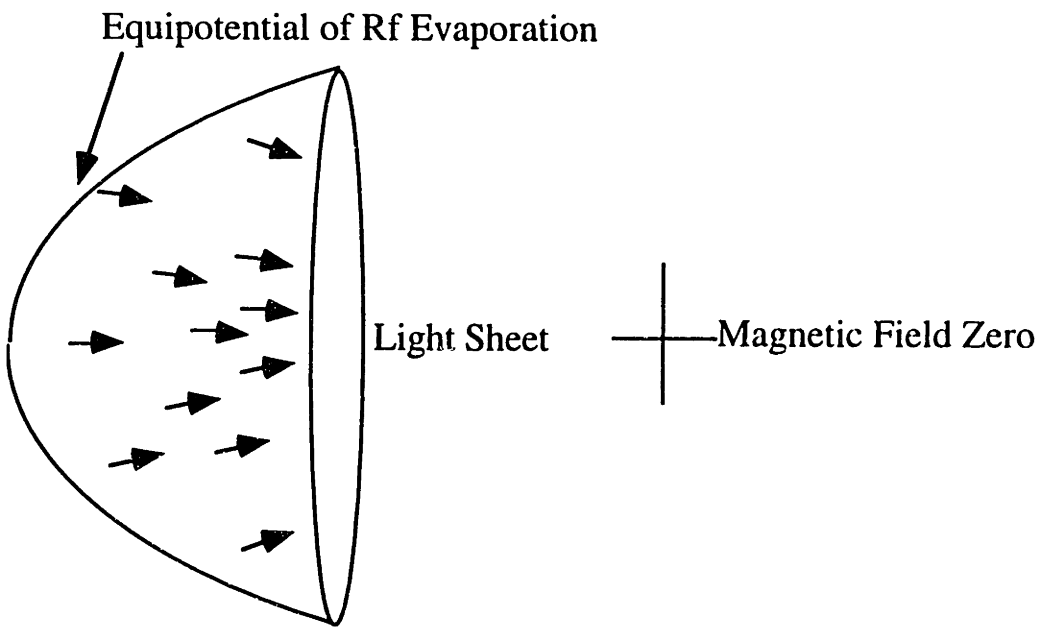

Figure 5.3 In the light sheet trap atoms are confined at a finite bias field, and are thus polarized predominantly along this direction., As a result Majorana spin flips are reduced by a big factor, and the trap becomes less sensitive to small errors in alignment.

There is one final advantage to the light sheet trap. Once the zero of the magnetic field has been displaced we have an alternate way to force the evaporation. A cloud can be displaced parallel to the light sheet by an appropriate bias field. If the light sheet has a sharp edge then the atoms with the highest total energy will spill over the edge of the light sheet and fall into the magnetic field zero (see figure 5.4).

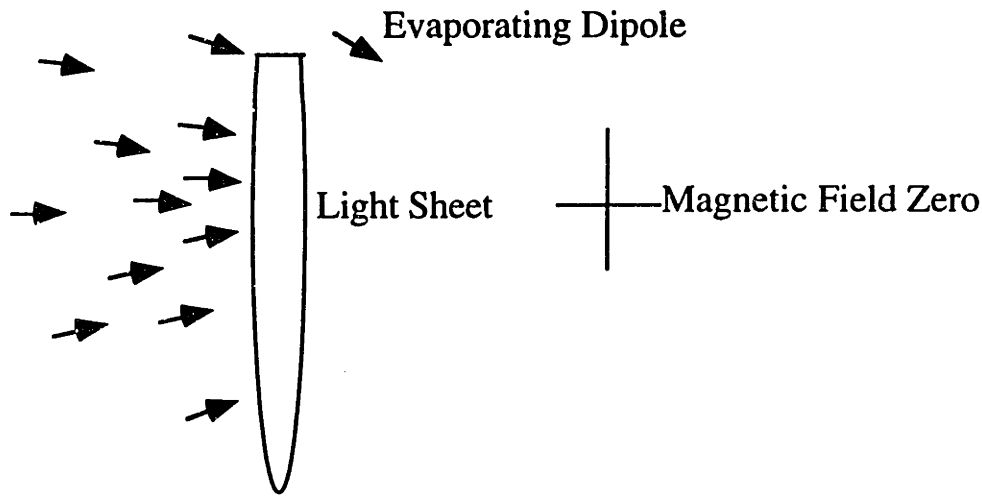

Figure 5.4 Evaporation of a very cold cloud with out rf. The asymmetric light sheet allows atoms with more that the average amount of total energy to escape and fall into the magnetic field zero.

5.2 Experimental Results

Our first experiment with the light sheet was a success. It was in fact no more difficult to align than the optically plugged magnetic trap and adiabatic decompression became trivial. After adiabatic decompression absorption images of the cloud were taken at various frequencies (see figure 5.5). A fit to the minimum transmission through the cloud is shown in figure 5.6.

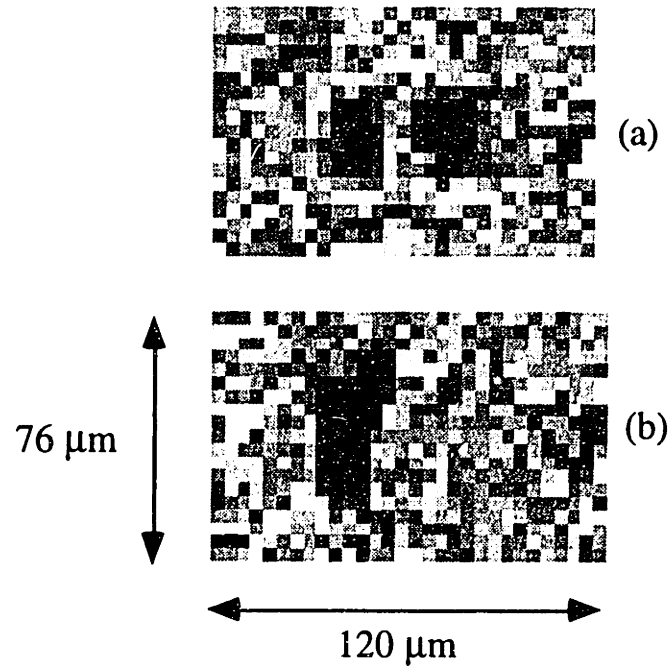

Figure 5.5 Absorption images taken in a light sheet trap. (a) Absorption image before displacement of the field zero and decompression and (b) image taken after decompression and displacement of the field zero.

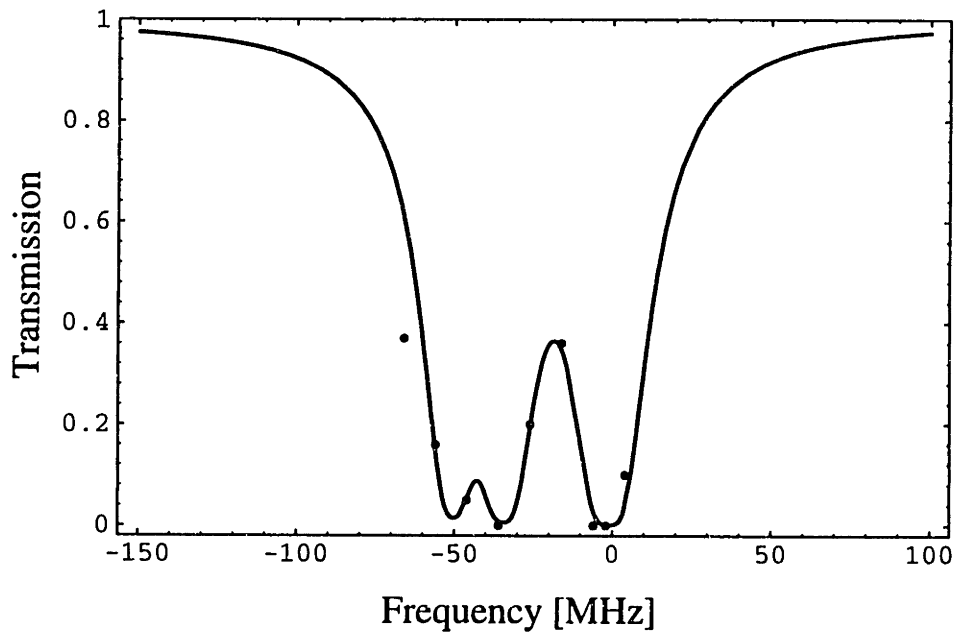

Figure 5.6 Absorption spectrum of a 20 μm cloud of sodium atoms trapped in a light sheet trap. The best fit yields an optical density of 6.5 which corresponds to an atomic density of 3×10^{12} cm^{-3} and ~ 10^4 trapped atoms.

An optical density of 6.5 and a 20 μm cloud imply a density of $3x10^{12}$ cm^{-3} and a temperature of 1 μK. This corresponds to a phase space density only one order of magnitude lower than required for the observation of Bose-Einstein condensation.

In phase space we have come a long way very rapidly, figure 5.7 shows the phase space path that we have taken to get so close to the transition point.

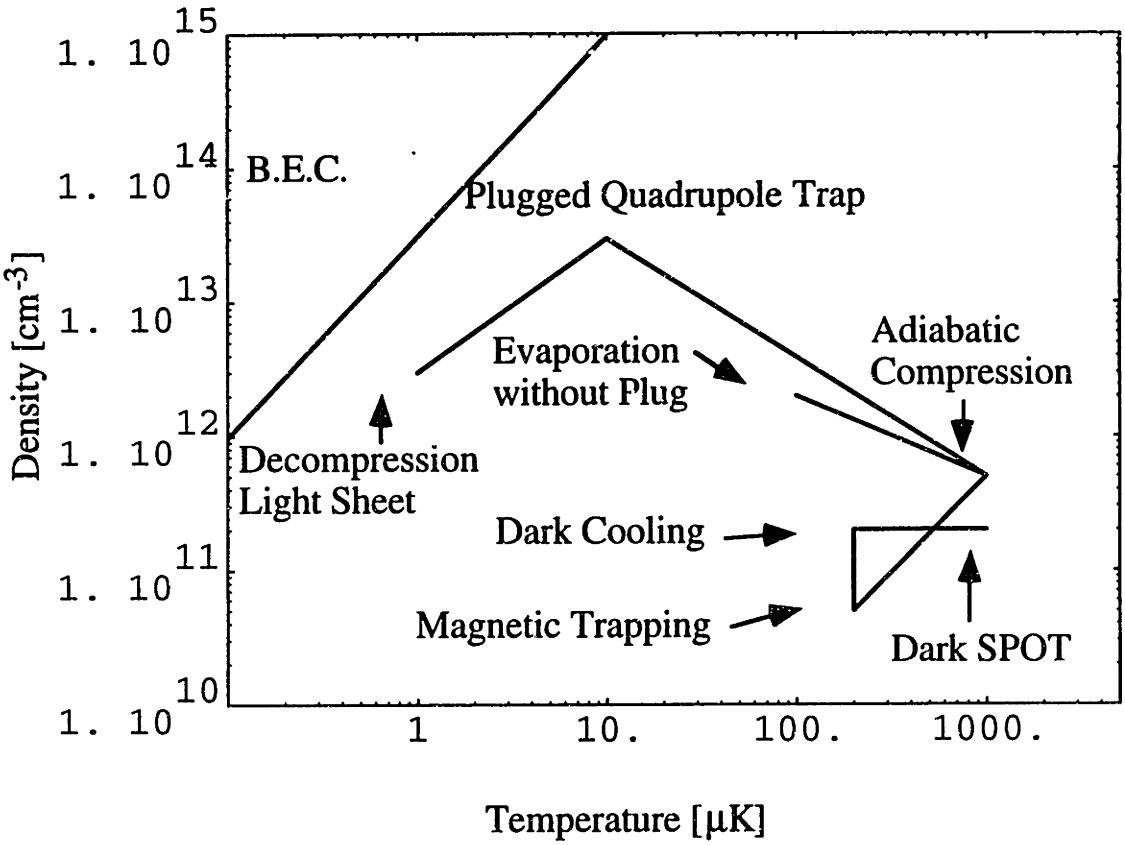

Figure 5.7 Phase space plot of our path towards Bose-Einstein Condensation.

Chapter 6
Suggestions for Future Work

Based on our preliminary results it seems that the light sheet trap provides an ideal potential in which to do further evaporation and hopefully to observe Bose-Einstein condensation. We were unable to push the experiment to the condensation line thus far because of some technical difficulties (these are in the process of being ironed out). As of now we know of no physical reason why we shouldn't be able to cross the transition line in the near future. This of course in no way implies that there isn't a limitation but at the very least it is not obvious.

Assuming that there is not a limitation and Bose condensation is achieved there are a number of experiments which should be done. The first of these experiments would obviously be to observe the reduced spatial extent of the condensate relative to the rest of the thermal cloud. Another preliminary experiment that we are already prepared to do would be to do laser spectroscopy on the condensate. This is of particular interest because, as was mentioned in the introduction, there is some theoretical uncertainty as to how the condensate will react to laser light.

There are other experiments which would also be of significance. Mapping out the transition line in phase space would allow us to test the validity of assumptions based on mean field theory. Also of particular interest would be to release the condensate into free space and observe the worlds first coherent source of atoms (a "Boser"). Atom interferometry with a Boser might prove to be a fruitful line of research.

There are also experiments relating to work done in liquid He which might shed some light on degenerate systems. For instance measurements of the viscosity and heat conductivity of the condensate as a function of density might allow us to explore regions where the quantum gas is more strongly interacting.

There are of course many unknowns in these lines of research and perhaps the only thing that can be said with certainty is that there are going to be a lot of very interesting results to follow!

References

1 K. Huang, *Statistical Mechanics* (Wiley, New York, 1987).

2 J. Javanainen, Physical Review Letters **72**, 2375 (1994).

3 M. Lewenstein and L. You, Physical Review Letters **71**, 1339 (1993).

4 J. M. Doyle, (Massachusetts Institute of Technology, 1991).

5 E. Raab, in *Physics* (MIT, 1988).

6 P. D. Lett, R. N. Watts, C. I. Westbrook, *et al.*, Physical Review Letters **61**, 169 (1988).

7 A. Aspect, E. Arimondo, R. Kaiser, *et al.*, Physical Review Letters **61**, 826 (1988).

8 N. Davidson, H.-J. Lee, M. Kasevich, *et al.*, Physical Review Letters **72**, 3158 (1994).

9 A. Kastberg, W. D. Phillips, S. L. Rolston, *et al.*, Physical Review Letters **74**, 1542 (1995).

10 M. Joffe, in *Physics* (M.I.T., Cambridge, 1993).

11 K. B. Davis, M.-O. Mewes, M. A. Joffe, *et al.*, in *Physical Review Letters*.

12 M. Kasevich, personal communication .

13 W. Petrich, M. H. Anderson, J. R. Ensher, *et al.*, in *Physical Review Letters*.

14 E. L. Raab, M. Prentiss, A. Cable, *et al.*, Physical Review Letters **59**, 2631 - 2634 (1987).

15 W. Wing, Progress in Quantum Electronics **8**, 181-199 (1984).

16 H. Hess, G. P. Kochanski, J. M. Doyle, *et al.*, Physical Review Letters **59**, 672 (1987).

17 C. Monroe, in *Physics* (University of Colorado, 1992).

18 R. Edge, The Physics Teacher **33**, 252 (1995).

19 Teisinga, Kuppens, Verhaar, *et al.*, Physical Review A **43**, 5188 (1991).

20 E. Tiesinga, A. J. Moerdijk, B. J. Verhaar, *et al.*, Physical Review A **46**, R1167 (1992).

21 H. F. Hess, Physical Review B **34**, 3476 (1986).

22 N. Masuhara, J. M. Doyle, J. C. Sandberg, *et al.*, Physical Review Letters **61**, 935 (1988).

23 W. Ketterle and D. E. Pritchard, Physical Review A **46**, 4051-4054 (1992).

24 C. Cohen-Tannoudji, *Atom-Photon Interactions* (John Wiley and Sons, Inc., 1992).

25 J. Rubbmark, Kash,M. et al., Physical Review A **23** (1981).

26 M. Andrews, (M.I.T., 1997).

27 T. W. Hijmans, Y. Kagan, G. V. Shlyapnikov, *et al.*, Physical Review B **48**, 12886-12892 (1993).

Acknowledgement

I would like to take this opportunity to thank some of the people who have helped me in one way or another during my graduate school years.

First and foremost I would like to thank my thesis advisor Wolfgang Ketterle who has been; a patient teacher, a trusted collaborator and a good friend. I would also like to thank my fellow graduate students Marc-Oliver Mewes and Michael Andrews who have contributed to this experiment in ways to numerous to mention. I wish all of them continued success.

I am also gratefui to past members of our group. Michael Joffe and Alex Martin where very helpful in my early years in the lab and taught me many of the basic techniques of experimental physics that were crucial to the current success of this experiment.

I would also like to thank several members of the Kleppner group. In particular special thanks goes to Robert Lutwak and Jeff Holley who have always been willing give excellent technical advice and also loan precious pieces of equipment. I would also like to thank Jeff for being, a reliable lifting partner, a considerate roommate, and a close friend (perhaps his only serious flaw is that he went to Williams). I would also like to thank my other roommate / fellow graduate student Hong Jiao whose enthusiasm for the Chargers and spaghetti is legendary.

I would like to acknowlege support during my first two years of graduate school from the MIT Compton Fellowship and during my fourth year from the MIT Wolfe Fellowship. I would also like to thank the department and Martin Deutsch for selecting me to be the recipient of the 1994 Deutsch prize.

I would like to thank my parents and siblings for their continued support and encouragement during the last five years. Finally I would like to thank Wendy for her

patience and support during the many long days and nights of work that resulted in this thesis.